# Experimental Investigation and Modeling of Sand Jets Passing through an Immiscible Layer

By

Niyousha Mohammadidinani

Supervisor: Dr. Amir H. Azimi

Co-supervisor: Dr. Siamak Elyasi

A Thesis Submitted to Department of Civil Engineering

in Partial Fulfillment of the Requirement for the Degree of

Master of Science

at

Lakehead University

Thunder Bay, Ontario, Canada

August 2016

# Abstract

Sand jets passing through two immiscible liquids, water and oil have many applications in the field of civil and environmental engineering such as tailings transport, dredging and discharge of industrial and urban wastewater. Understanding the dynamic interactions of the sand particles and its ambient are important for proper design and optimizing the engineering systems. Mass, momentum and energy of the system can be influenced by interactions of the suspended particles within the jet. The conducted experimental studies and numerical and nominal modeling in this thesis are new in terms of the fundamental understanding of jet characteristics.

Part of this thesis focused on the experimental parameters and characteristics of oily sand jets such as frontal width and velocity. Effects of the controlling parameters of the oily sand jets such as nozzle diameter, oil layer thickness and mass were investigated and it was found that the effect of nozzle diameter on evolution of oily sand jets was more significant than the other parameters.

Study in water phase, it was observed that the bursting of a group of particles covered with a thin oil layer can be classified into three different forms. Evolution of trailing waves of the oily sand jets and their characteristics such as wave length and wave amplitude were also investigated.

Part of this thesis focused on Data mining and boundary visualization techniques to study the effects of experimental parameters on the shapes of oily sand jets. Model trees were developed to classify and predict the growth of oily sand jets at different conditions. It

was found that the model tree can predict the growth of sand jets with an uncertainty of ±8.2%, ±6.8% and ±8.7% for width, velocity and distance from the nozzle, respectively.

The main aim of this thesis is to explore and find correlations between the dynamics of sand particles through passing oil-water interface and controlling parameters such as nozzle diameter, oil layer thickness and mass of sand particles. Therefore, it was found that the nozzle size has significant effect on characteristics of evolution of oily sand jets such as frontal velocity, development of bursting, formation of trailing wave section and shear stress in comparison with other controlling parameters such as oil layer thickness and mass of sand particles. Investigation of formation of frontal shapes of oily sand jets in water indicates the fate of sand jets after passing an immiscible interface and sedimentation of sand particles. The main controlling parameter for evolution of various shapes of oily sand jets front is the nozzle diameter. Mass of sand particles and oil layer thickness are the secondary and tertiary important parameters. Evolution of different frontal shapes of oily sand jets can also change specific characteristics of oily sand jets such as frontal velocity and width. In terms of environmental analysing formation of various shapes of oily sand jets can explain variations of velocity of sediments and under which conditions these sediments spread or deposit without dispersion in oceans.

# Acknowledgements

I would like to offer my sincerest gratitude to my supervisor, Dr. Amir Hossein Azimi, who has always been supportive throughout my thesis with his patience and knowledge. I attribute the level of my Master degree to his encouragement and effort, without him this work would not have been completed. One simply could not wish for a better or friendlier supervisor.

I am grateful to all my professors at Lakehead University and the NSERC-Discovery grant for their helps and encouragements.

I would also like to thank all my friends and colleagues at Lakehead University especially Neda Mehrvarz, Mohammad Moghadaripour, Masoud Manzoori, Sadra Mesbah and Mona Amiri who are always willing to help and give their best suggestions throughout my work.

My special gratitude goes to my family for their understanding, affection and support all throughout the years. My parents who have always been supporting and encouraging me through all the challenges of my life for which I am eternally grateful. My sister and her husband for supporting me for everything and giving me pieces of advices which can helped me overcome many obstacles.

# Table of Contents

# List of Figures

# List of Tables

**Chapter 1**

# General Introduction

## 1.1 Motivation and Background

Canada's reserves have third place in the world. Over 95% of these reserves are in the oil sands deposits in the province of Alberta (Energy Information Administration, 2007). Alberta is one of the largest oil deposits in the world with a reserve of 174 billion barrels of bitumen. In recent years technological breakthroughs have overcome the economical and technical difficulties of producing the oil sands and by 2007 %64 of Alberta's petroleum production of 1.86 million barrels per day (296,000 $m^3$/d) was from oil sands rather than conventional oil field (ERCB). Since oil-sand mines consume large volumes of water (i.e. 1 $m^3$ of water for 1 barrel of oil) and the intake of freshwater from rivers is limited to less than 2% of the annual flow, oil-sand operators have to store the processed waters and tailings on-site to recycle and reuse. The oil-sands tailings contain between 70 to 80 % of water and approximately 20-30% of solid materials.

The reclamation processes of tailing ponds can be achieved by many techniques such as capping the fine residuals and wastes by a layer of sand to preserve ecosystem similar to its original landscape. One of the most difficult environmental challenges is managing volume of tailings in oil-sand tailing ponds. A major problem is identification of mixture of compounds and dynamics of sediments in these ponds. By study the dynamics of sand jets passing through an immiscible layer it can be possible to estimate the dynamic, mixing and spreading of those sediments under the oil-water interface.

**Figure 1-1:** Oil sand flows dispose into tailing ponds.

(http://priceofoil.org/2014/02/24/tar-sands-tailing-ponds-leaking/)

Geophysical buoyant jets resulting from temperature or salinity differences can occur in the ocean and in magma chambers near the crust of the earth.

**Figure 1-2:** Magma flows enter to the ocean.

(http://www.shutterstock.com/)

Magma is a complex high-temperature fluid with a mixture of molten or semi-molten rock, volatiles and solids and it forms a gravity driven solid-liquid jet or thermal when enters into a water. Since is difficult to study dynamics of gravity-driven magma flows in water due to natural limitations, however, different experimental conditions can be set to model these types of flows. The present experimental study aims at investigating the dynamics of sand jets passing through an interface between two immiscible liquids. The presented methodology and the obtained results can be employed to understand the dynamics of sand particles in tailing ponds and magma flows in ocean.

Two-phase flows can be formed by introducing a disperse phase (i.e., solid, liquid or gas) into a continuous phase (i.e., liquid or gas). Solid-liquid flows can form a jet known as sand or slurry jets (Hall et al., 2010).

**Figure 1-3:** Image of sand jet passing through 4mm nozzle diameter in water.

These types of flow have many applications in the field of civil and environmental engineering such as tailings transport, dredging, discharge of industrial and urban wastewater (Azimi et al., 2012a, 2012b, 2014, 2015).

**Figure 1-4:** Image of dredging.
(http://www.imdc.be/taxonomy/term/50)

**Figure 1-5:** Image of discharging industrial and urban wastewater.
(http://inweh.unu.edu/wastewater-reuse-infographic/)

When amount of mass injected into liquid, a sand jet forms and penetrates to a certain length and then breaks up into many particles. Suspended particles play a major role in the ecology and pollution of environmental systems such as oceans and atmosphere. Understanding the dynamic interactions of the sand particles and its ambient is important for efficient design and for optimizing the engineering systems.

As a result, particle motion and the surrounding fluid velocities, turbulence, and the shear stresses are affected by particle interaction mechanisms. The interaction between two phases enhances the complexity of the system and mixing phenomenon.

A recent practical example of flow of sand jets and thermals through an immiscible oil-water interface can be found in oil-sand tailings ponds where the water in tailings pond is covered by a thin layer of bitumen and residual oil. Limited research investigations have been devoted to study the dynamics of sand jets passing through immiscible liquid layers.

A number of studies focus on the impingement of a stratified miscible interface (Baines 1975 and Noh et al.,1992). Philippe et al., (2005) studied the negatively buoyant jets injected in a miscible liquid. They found that after an initial intrusion phase, the jet reaches a steady-state by a constant penetration depth. Researches on immiscible interfaces impinged with a jet focus on mixing mechanisms, Froude number and Richardson number.

Friedman and Katz (1999) investigated the effects of water jets impinging into a water and diesel layers. They observed four distinct flow regimes in their experiments and correlated their results and classifications with Richardson number, $\mathrm{Ri}=(\rho_w-\rho_{oil})\, d_o g/(\rho_s u_o^2)$ where $\rho_{oil}$ is the density of oil (fuel), $g$ is acceleration due to gravity and $u_o$ is the initial jet velocity and $d_o$ is the nozzle size. Webster and Longmire (2001) investigated the behaviour of glycerin-water jets flowing into immiscible ambient. They found that the forcing frequency and the viscosity ratio between fluids had a strong effect on the flow regime and pinch off characteristics.

Particle-laden jets are commonly observed when particles are released instantaneously into water bodies such as aqueous industrial waste disposal (Buhler and Papantoniou, 1991; Bush et al., 2003).

Less attention has been devoted to study of the fronts of sand jets passing through an immiscible interface. The shape, frontal velocity and width of oily sand jet are related to many parameters which are investigated experimentally in this thesis.

## 1.2 Objectives

The major purpose of investigation of this study is to understand the hydrodynamics of oily sand jets in water to simulate oil sand tailing ponds. Sediment management and handling the flow of slurries in these tailing ponds is one of the most environmental obstacles. By considering an oil layer in water surface it can be estimate how fast these sediments grow under this immiscible interface.

Since it is difficult to study the dynamics of magma flows and also it is impossible to create molten materials near magma's temperature, attempt was made to create conditions which were similar to movements of magma when falling in water of oceans. Understanding and analysing the dynamic of evolution of oily sand jets frontal shape can help explaining the mechanisms of heat transfer from molten materials into water ambient. Depending on the shapes of magma flows impinged into water interface, the molten material can lose their heat gradually or rapidly. If one of the oily sand jets shapes that I considered such as bursting or separation to many small groups of particles occurs, maybe the molten materials transfer the heat to the ambient earlier.

## Chapter 2

# Literature Review

Limited research investigations have been devoted to study the dynamics of sand jets passing through an immiscible liquid layer. A number of studies examined Newtonian liquid jets into Newtonian or non-Newtonian liquids including jet instabilities, breakup length and drop formation.

Cai et al., (2012) studied the sand jet behavior in non-Newtonian viscoplastic fluid. They investigated deformation regimes of sand jets by depositing circular sand jets vertically into viscoplastic fluids, known as Laponite gel. They found various regimes such as dripping, jetting and mixing for sand jets. These regimes are proportional to entry velocity, size of the jet and viscosity of the fluid. Williamson et al., (2008) examined the behavior of fountains (negatively buoyant jets) by injecting salt water up into a fresh water tank by using various nozzle diameters ($d_o$=4.80, 2.54,1.66, 1.13, 0.76 and 0.54 mm). They studied the behaviour of fountains over a wide range of Froude $\mathrm{Fr}=u_o/(R_o g')^{1/2}$ ($0.7<\mathrm{Fr}<100$) and Reynolds $\mathrm{Re}=u_o R_o/\nu$ ($15<\mathrm{Re}<1900$) numbers where $R_o$ is the radius of the source, $u_o$ is the initial velocity, $g'$ is the reduced gravity and $\nu$ is the kinematic viscosity of the fluid, from weak to strongly forced flow and from laminar to fully turbulent flow. They observed several unstable modes and formed a regime map based on Froude and Reynolds numbers. They identified a number of sub-regions where the behaviour varied significantly with both Reynolds and Froude numbers for weak laminar fountains. They also found that the flow has a Reynolds number dependence in all

laminar and transitional regions. They observed the sinuous instability for both low and high Reynolds number.

Most of existing literature focused on the behaviour of sediment-laden jets and slurry jets in water. Slurry jets can be found in many industrial and environmental application such as in hydro-power systems, wastewater disposal, stirring vessels and marine bed capping. Experimental studies of slurry jets have indicated that many parameters such as particle size, $D_{50}$, particle concentration, $c_o$, initial jet velocity, $u_o$, and nozzle diameter, $d_o$, are important. Some experimental investigations were successful in partially measuring the characteristics of highly concentrated slurry jets.

Hall et al. (2010) studied turbulent sand jets and sand-water slurry jets impinging vertically into a stagnant water. They measured sand-phase velocity and concentration of slurry jets with small particle size ($D_{50}$=206μm). They investigated the dynamics of sand and slurry jets with an initial sand volume fraction of $c_o$=0.6. The initial volumetric concentrations for slurry jets were varied from 0.055 to 0.124. Nozzle diameter of ($d_o$=6.1, 10.3 mm) and ($d_o$=15.5, 9 mm) were used to form the sand jet and slurry jet, respectively. The concentration and velocity found to have self-similar Gaussian profiles. It was found that the centerline sand concentration decayed with a −5/3 power relation and the centerline particle velocity decayed with a rate of −1/3, similar to a single-phase plume. They found the terminal velocity varied depending on sand mass flux and the spreading rates of the jets varied with the particle Froude number $\mathrm{Fr}=u_o/(gd_o(\rho_s-\rho_w)/\rho_w)$ where $\rho_s$ and $\rho_w$ are the density of sand and water, respectively, $d_o$ is the jet diameter, $u_o$ is the average velocity at the water surface and $g$ is the gravitational acceleration. The evolution of a laminar liquid jet injected with negatively buoyant condition in a miscible

liquid was studied by Philippe et al., (2005). The flow rate $Q$ was varied from 0.002 $cm^3/s$ to 20 $cm^3/s$. Seven different diameters were used ($d_o$=0.254, 0.407, 0.508, 0.838, 1.372, 1.75 and 4.83 mm) to cover wide range of Reynolds number. They designed a simple theoretical model which predicted the transient phase and steady phase in terms of penetration depth and jet's profile.

To estimate the axial particle velocity of the slurry jets, Jiang et al. (2005) proposed a correlation based on the summation of the fluid velocity and the settling velocity of particles, used fluorescent glass beads and polyamide particles. The formulation was obtained based on the experimental study of low concentrated (0.19%) slurry jets with 75 μm particles. They indicated that the centreline velocity of sand-phase is higher than the water-phase and can be predicted as the summation of the water-phase velocity and particle settling velocity.

Particle volume fraction has a prominent role in the structure and behaviour of the solid-liquid jets. Investigation on the effect of particle volume fraction indicates that by increasing the volume fraction of the particle phase, the spreading rate of both phases will increase (Virdung and Rasmuson, 2007). The results were obtained from experimental and numerical study of solid-liquid jets with low volume fractions (less than 2%). Sheen et al. (1994) conducted a series of experiments to study the effect of particle size on solid-gas turbulent jets. Polystyrene particles of 210, 460 and 780 μm were used with the mass loading ratio (i.e. ratio of particle mass flux to the gas/fluid mass flux) ranging from 0 to 3.6 ($c_o$≈0.43%). They found that for $x/d_o$>10, the decreasing of the centerline axial velocity for the two-phase jet flow is smaller than that of the corresponding single-phase

jet. They also reported that the turbulent intensity of the jet increases by increasing particle size and decreases by increasing particle concentration.

The unsteady behaviour of particle-laden jets/plumes and the evolution of particle cloud can be classified into different regimes by introducing some critical parameters such as particle Reynolds number, and particle Froude number. In the release of a fixed amount of particles in stagnant water, the evolution of particle cloud and its velocity were correlated with the buoyancy force exerted by the particles whereas the frontal evolution of a continuous release of particles can be correlated with the buoyancy flux of the jets [Noh and Fernando (1993); Noh (2000) and Bush et al. (2003)]. The behaviour of these jets is determined by the size, concentration and density of the suspended particles. Nicolas (2002) classified the settling of particle cloud in water and glycerine into four different regimes: stable jet, unstable jet with blobs formation, spiral jet with dispersion and atomized jet. The tube diameters $d_o$ were ranging from 4 to 8 mm to form a jet. He found that a capillary-like instability with formation of blobs and dispersion of the jet particles occur when a particle Reynolds number is over unity when liquid inertia becomes dominant over the viscous force and the particle Reynolds number is a good criterion to characterize the dispersion phenomenon. He also found that the hydrodynamics bonds between particles are strong enough to keep the jet in a cylindrical shape. He compared the shape of a liquid-into-liquid jet (dyed glycerol into salted water) to a suspension jet (polystyrene particles into water) and observed cylindrical and very stable shape for the liquid-into-liquid jet and found that the contrast of viscosity cannot explain the suspension jet instability.

The physical mechanisms and the characteristics of the cloud of particles as it descended in the water column were investigated by Ruggaber (2000). In his experiments effects of practical release parameters such as release location (i.e., release height) and moisture content were investigated. He found that the thermal phase of particle clouds can be subdivided into turbulent thermals in the absence of spherical vortex and circulating thermals in the presence of vortices. Bush et al., (2003) examined settling of particle clouds in homogeneous and stratified ambient flows with particle Reynolds numbers ranging from 0.1 to 300. They also investigated the condition under which the particle cloud settles as a thermal or as a swarm of individual particles. The dependence of the normalized cloud velocity on the normalized buoyancy force of a particle cloud was correlated and it was found when the normalized buoyancy is less than 0.1, particles descended as a swarm of individual particles and for the normalized buoyancy above 0.1, settlement of particles behaved as thermal. Rogers and Morris (2009) studied the scaling and morphology of buoyant jets in laminar regime and spanned a wide range of plume Richardson numbers. They found that plume's morphology and speed eventually become independent of buoyancy and momentum. They observed confined and unconfined plume heads for large and small Richardson numbers, respectively.

Studies on sand jets in air have been the topic of research in the past. Experimental study of circular sand jets in air from three nozzles diameter ($d_o$=19.2, 31.1 and 63.8 mm) with different sand particle sizes ($D_{50}$=0.21, 0.38 and 0.52 mm) was examined by Cai et al., (2010). It was found that the frontal speed of these sand jets increases with the distance and its variation is independent of the dimension of the nozzle and the size of sand particles. While Azimi et al., (2012a) studied the behaviour of sand jets front in water

with different sand particle sizes (0.1375 mm≤ $D_{50}$ ≤0.507 mm) and nozzle diameters ($d_o$= 2, 3, 4.75 and 10 mm). They investigated the effect of nozzle size and particle size on the mean and turbulence of the frontal of highly concentrated slurry jets by measuring sand-phase velocity field. They found that the jet frontal velocity is a function of nozzle diameter and particle size and the particle grouping effect enhances the axial velocity and changes the growth rate of the particle cloud.

It has been theoretically and experimentally established that the width of single phase jets grows linearly with the axial distance of $x$ from the nozzle [Fischer et al., (1979) and Lee and Chu (2003)]. Observations on the growth rate of particle cloud close to the nozzle indicated a linear relationship between the width of the particle cloud and $x$. This relationship becomes non-linear far from the nozzle and the growth rate decreases until the particle cloud reaches the swarm condition [Bush et al., (2003); Noh and Fernando (1993), and Azimi et al., (2012a)].

An interesting flow feature that has long been associated with starting jets is the formation of vortex structure. The formation of the vortex is largely due to the roll up of the jet shear layer as it is introduced into the ambient. The generation, formation, and evolution of vortex rings have been the subject of numerous experimental, analytical and numerical studies [Garib et al. (1998); Krueger and Gharib (2003); Arakeri et al. (2004); Pottebaum and Garib (2004); Bond and Johari (2005 & 2010)]. Bond and Johari (2005) examined the effects of the initial geometry on the development of buoyant thermals. The flows were produced by releasing buoyant fluid (a solution of potassium dihydrogen phosphate in water) into a mixture of glycerol and water. They found significant correlations between thermal-like characteristics by releasing buoyant fluid from

cylindrical tubes of $L/d_o$ ratios 2 to 8 into a uniform density environment and the higher aspect ratio leads to higher circulation. The impact of buoyancy on the development of vortex ring was examined by Bond and Johari (2010). The vortices were formed in a water tank with cylindrical tube of $L/d_o$=2. They found that the vorticity in the core of buoyant and non-buoyant vortex rings is symmetric and has a Gaussian distribution.

Pantzlaff and Lueptow (1999) investigated the initial transient character of both negatively and positively buoyant jets into homogeneous fluids. They considered only situations where the momentum of the jet is significant. The fluids used as jet and bulk liquid were water and aqueous potassium chloride (KCl) solutions. The momentum is the primary factor in determining transient for positively buoyant jets. They observed several different flow structures depending upon the buoyancy and momentum of the jet. They also found that the jet penetrates to the free surface of the tank and does not become plume-like due to higher initial momentum at high Reynolds number (2500<Re<15000). At low Reynolds number the jet fluid simply overflows the tank and the mixing of jet fluid with ambient is not strong.

Laboratory experiments of two-dimensional thermal (salt solution) released at the upper surface of a two-layer (saltwater underneath a layer of freshwater) stratified fluid were investigated by Noh et al., (1992). They used a half-cylinder of $d_o$=5cm to generate the two-dimensional thermal. They observed two distinct flow regimes. The initial thermal was observed to be similar of a vortex pair and subsequent evolution of the flow was found to be dependent on the Richardson number of the interface after impingement $\mathrm{Ri} = l\Delta b / w^2$ where $l$ and $w$ are the length and velocity scales of the thermal and $\Delta b$ is the buoyancy at the interface.

For engineering assessment, good understanding is required in order to accurately place the sediments in a targeted area, as well as to address the loss of sediment to water body which results in turbidity and associated water quality impacts. Zhao et al., (2012) investigated the underwater behaviour of sediment thermals, formed by releasing dry sediments instantaneously from various heights above water. They focused on lifting sediments to a certain height above the water and then releasing them freely. In this manner the sediment cluster travels through air, accelerates and garners significant momentum before impacting the water surface. They observed that the penetration rate decreased as the air release height increased.

Some researchers investigated the dynamics of single-phase jets passing through immiscible layers in the past. Friedman and Katz (1999) focused on the structures of a fuel and water interface when impinged with a water jet for $90>\mathrm{Ri}>0.01$ and $30000>\mathrm{Re}>1000$. They identified four distinct flow regimes in their experiments and correlated their results and classifications with Richardson number, $\mathrm{Ri}=(\rho_w-\rho_{oil})d_o g/(\rho_s u_o^2)$ where $\rho_{oil}$ is the density of oil (fuel), $g$ is acceleration due to gravity and $u_o$ is the initial jet velocity and $d_o$ is the nozzle size. They found that the transitions between regimes are entirely Ri dependent, however, the onset of droplet formation is dependent on both Ri and Re numbers. Geyer et al., (2011) investigated the dynamics of negatively buoyant jets in a homogeneous immiscible ambient fluid. They injected colored water into a cylindrical tank containing rapeseed oil and kept the inlet flow rate constant over the duration of their experiment. The volume flow rate ($0.9\ \mathrm{cm^3/s} < Q < 42\ \mathrm{cm^3/s}$) and nozzle diameter ($2.4\ \mathrm{mm} < d_o < 11\ \mathrm{mm}$) were varied to cover a wide range of Reynolds ($468<\mathrm{Re}<5928$) and Richardson ($8\times10^{-4}<\mathrm{Ri}<1.98$) numbers. They

found three distinct flow regimes as very stable, oscillatory, smooth and wavy. Friedman and Katz (2000) measured the maximum penetration depths for two flows. For the first flow, the jet travels through an identical fluid before reaching a sharp density interface, where negative buoyancy slows it down until the jet reaches a maximum penetration depth. In this case, they measured the penetration depth from the elevation of the undisturbed interface. For the second flow, a fountain is injected directly into a fluid with a different density and the penetration depth is measured from the jet exit. They found that the penetration depth is only a function of a Richardson number and the penetration number is independent of Reynolds and Weber numbers in turbulent flow.

One of the fundamental phenomenon in fluid dynamics involves changes in the topology of interfaces between immiscible fluids. Common examples of topological changes are pinch-off of a continuous jet into droplets and droplet reconnection. The dynamics of topological transitions are difficult to characterize for several reasons such as fluid properties, like density, viscosity and interfacial tension. The behavior glycerin-water jets flowing into immiscible ambient was investigated by Webster and Longmire (2001). Two fluid combinations were studied with similar density ratios ($\rho_j/\rho_o$=1.18) where $\rho_j$ and $\rho_o$ are the jet and ambient fluid density but different viscosity ratios ($\mu_j/\mu_o$=0.152, 0.0077). It was found that the viscosity ratio affected the jet stability as well as pinch-off angles and drop size.

Dispersions of particles in large volumes of liquid are of interest for many industrial applications or natural phenomena. The dispersion of a collection of particles is relevant to many natural phenomena such as pyroclastic flows (i.e. fast-moving currents of hot gas and rock fragments produced by a volcanic eruption), turbidity currents (i.e. sediment-

laden flows) and the mixing and spreading of pollutants in lakes and oceans. When the particles are small or the liquid highly viscous, interactions between particles are governed by hydrodynamic forces. These forces lead to complex chaotic displacements of the particles. Metzger et al., (2007) examined the nature of the breakup of a cloud of particles falling in a viscous fluid. Clouds were produced by injecting the desired volume of suspension with quiescent fluid. They found that the evolution of a falling spherical cloud depends on the initial number of particles and the initial spherical cloud is unstable and evolves into a torus which breaks up into two droplets. They have characterized the systematic evolution toward a torus by measuring the evolution in time of the horizontal radius and the velocity of the cloud. They measured the percentage of particles that have escaped the cloud as a function of time and found good agreements between their experiments and simulations and found two regimes with two different rates of leakage. The rate of leakage was large when the cloud had sphere shape while the rate became small due to the evolution of the cloud into a tours shape.

Pignatel et al., (2011) examined the dynamics of a cloud of particles at a small Reynolds number in which macro-scale inertia and micro-scale inertia become dominant. They identified two inertial regimes and observed the cloud is flat and transits into a torus which further widens and eventually breaks up into droplets in both inertial regimes.

Many explosive volcanic eruptions are characterized by turbulent jets that ultimately deliver dense mixtures of gas and ash into the atmosphere. A major effect of this process is that the jet can become less dense than the atmosphere and rise as a buoyant plume to a level of neutral buoyancy. At this attitude (20-50 km) the mixture spreads as a turbulent gravity current and forming an umbrella cloud. Sedimentation of ash and pumice from

these clouds presents a number of potentially severe hazards such as roof collapses, or blockages of drinking water, waste disposal and power distribution systems. Carazzo and Jellinek (2012) investigated the evolution of umbrella cloud by simulating laboratory experiments of particle-laden jets with reversing buoyancy. They injected a well-stirred mixture of fresh water and well sorted particles into a tank with thick layer of salt water and overlying of fresh water. They observed different phenomena that occurred for varied initial volumetric flow rate and particle volume fraction. For low particle concentrations and relatively high flow rates, the mixture of solid particles and fresh water mixed rapidly with the ambient salt water layer. Although the particle laden jet was denser than the surrounding fluid, its density decreases as a result of turbulent entrainment and dilution to values lower than the ambient density. They found that the particle-laden umbrella clouds follow unexpected dynamical regimes depending on the flow intensity, the strength of the initial environmental density stratification and the particle concentration.

Chapter 3

# Experimental Investigation of Sand Jets Passing through an Immiscible Layer

## 3.1 Introduction

Two-phase flows can be formed by introducing a disperse phase (i.e., solid, liquid or gas) into a continuous phase (i.e., liquid or gas). The dispersion of particles in solid-liquid flows is relevant to many natural phenomena such as turbidity currents and sediment-laden flows in lakes and oceans (Pignatel et al., 2011). Solid-liquid flows can form a jet known as sand or slurry jets (Hall et al., 2010). Once a certain mass of particles releases into water it can form a particle cloud known as thermal (Noh and Fernando, 1993; Noh, 2000; Rahimipour and Wilkinson, 1992; Bush et al., 2003). These types of flow have many applications in the field of civil and environmental engineering such as tailings transport, dredging, discharge of industrial and urban wastewater (Azimi et al., 2012a, 2012b, 2014, 2015). In some cases, spreading of sand phase in sand jets or slurry jets becomes very limited due to natural conditions such as magma flows (Giraut et al., 2014). Once magma enters in to the water, it usually forms a gravity driven solid-liquid jet or thermal with a noticeable density difference. It is difficult to study dynamics of gravity-driven magma flows in water due to natural limitations, however, different experimental conditions can be set to model these types of flows. A recent practical example of flow of sand jets and thermals through an immiscible oil-water interface can be found in oil-sand tailings ponds where the water in tailings pond is covered by a thin layer of bitumen and residual oil. The processed oil-sand contains high concentration of fine sediments. The oil-sand effluent is discharged into tailing ponds to deposit sand

particles and reclaim the processed water. The present experimental study aims at investigating the dynamics of sand jets passing through an interface between two immiscible liquids. The presented methodology and the obtained results can be employed to understand the dynamics of sand particles in tailing ponds and magma flows in ocean. Limited research investigations have been devoted to study the dynamics sand jets passing through immiscible liquid layers. Most of existing literature focused on the behaviour of sediment-laden jets in water. Brush (1962) studied the momentum transport and spreading of solid and fluid phases in slurry jets. He found that the spreading rates are a function of particle size. Brush's results were confirmed experimentally from the study of sand-jets in water (Mazurek et al., 2002). Singamsetti (1966) observed that the velocity of the solid phase (i.e., sand) in sand-jets followed a self-similar Gaussian distribution. Nicolas (2002) conducted laboratory experiments to study the flow of gravity-driven jets of a dense suspension into a quiescent liquid. Four different flow regimes were observed to characterize the dispersion phenomenon based on non-dimensional parameters. Hall et al. (2010) investigated the dynamics of sand and slurry jets with an initial sand volume fraction of $c_o$=0.6. The initial volumetric concentrations for slurry jets were varied from 0.055 to 0.124. It was found that the centerline sand concentration decayed with a −5/3 power relation and the centerline particle velocity decayed with a rate of −1/3, similar to a single-phase plume. Experimental studies on the behaviour of sand jets front in water with different sand particle sizes (0.1375 mm≤ $D_{50}$ ≤0.507 mm) and nozzle diameters ($d_o$= 2, 3, 4.75 and 10 mm) was examined by Azimi et al. (2012a). It was found that the jet frontal velocity is a function of nozzle diameter and particle size. Shapes and formation of the frontal head were classified based on particle

Reynolds number, $Re_p=\rho_w u_\infty D_{50}/\mu$ where $\rho_w$ is the density of water, $u_\infty$ is the terminal settling velocity of sand particles, $D_{50}$ is the mean sand particle size and $\mu$ is the dynamic viscosity of water. It was found that the frontal head behaved as a thermal for $Re_p<10$. For $Re_p\geq10$ the sand jet front became narrower and vortex ring became weaker.

Dynamics of single-phase jets passing through immiscible layers have been the topic of research in the past. Friedman and Katz (1999) investigated the effects of water jets impinging into a water and diesel layers. They observed four distinct flow regimes in their experiments and correlated their results and classifications with Richardson number, $Ri=(\rho_w-\rho_{oil})\ d_o g/(\rho_s u_o^2)$ where $\rho_{oil}$ in the density of oil (fuel), $g$ is acceleration due to gravity and $u_o$ is the initial jet velocity and $d_o$ is the nozzle size. Geyer et al. (2011) investigated the initial upwards motion and fountain formation of a negatively buoyant jet flow in an immiscible ambient fluid. They used fresh water as a jet flow and rapeseed oil as an ambient fluid. Flow regimes and criteria for collapsing of negatively buoyant jets were defined using relevant non-dimensional parameters. Bush et al., (2003) examined settling of particle clouds in homogeneous and stratified ambient flows with particle Reynolds numbers ranging from 0.1 to 300. They found that particle deposition in a stratified fluid depends on the thickness of the top layer, fall out height and the intrusion height of the thermal. Many experimental and numerical studies have been carried out to investigate the dynamics of sand and slurry jets. However, less attention has been devoted to investigate the behaviour of sand jets in water after passing through an immiscible (i.e., oil-water) layer. Once particles passed the upper oil layer, they are covered with a thin film of oil. Particle encapsulation by a thin oil layer prevents the spreading of sand particles and completely affects the dynamics of sand particles in

water. Once oily sand jets descent into water, they may partially breakdown or spread due to rupture of the oil film. Preliminary observations indicated that the oil layer thickness, mass of sand particles and nozzle size are the dominant controlling factors. Different frontal shapes were observed representing the impact of different controlling parameters on formation of oily sand jets. Flow parameters such as distance from the nozzle $x$, frontal width $w_f$ and frontal velocity $u_f$ can be predicted if the relationship between parameters are known.

The present research work attempts to explore and find correlations between the dynamics of particles in an oily sand jets and controlling parameters. This study is organized in 5 sections. Section 3.2 presents dimensional analysis to find important parameters to study particle dynamics through immiscible interfaces. In section 3.3 experimental setup and techniques are discussed. Experimental results are discussed in section 3.4. Summary and conclusions of the present study is explained in section 3.5.

## 3.2 Dimensional Analysis

Dimensional analysis was found to be an effective tool to understand phenomena dealing with many variables. Dimensional analysis groups related variables to form non-dimensional parameters and evaluates the controlling forces, length and time scales. Parameters that may control the motion of sand jets passing through an immiscible layer such as frontal velocity $u_f$ can be identified as:

$$u_f = f_1 (x, \rho_s, \rho_{oil}, \rho_w, d_o, D_{50}, h_{oil}, u_o, g, c_o, t, m) \quad (1)$$

where $x$ is the axial distance from the nozzle, $\rho_s$ is the density of sand particles, $h_{oil}$ is the thickness of oil layer, $u_o$ is the initial velocity of sand jets, $t$ is time, $m$ is mass of sand

particles and $c_o$ is the initial volumetric concentration of particles. The volumetric sand concentration in this study was constant (i.e., $c_o$=0.6). Mass of sand particles can be converted into a length scale ($L$) is an equivalent tube length filled with sand particles.

$$L = \frac{4m}{c_o \rho_s \pi d_o^2} \tag{2}$$

Bond and Johari (2005) found a relationship between the frontal velocity and $L/d_o$. The $L/d_o$ ratio in this study is ranging from 1.02 to 326.51. Assuming constant density for sand particles, oil, and water and uniform particle sizes, the remaining parameters from Eq. (1) can be grouped together to reduce the number of non-dimensional parameters as

$$\frac{u_f}{u_o} = f_2\left(\frac{x}{d_o}, \frac{h_{oil}}{d_o}, \frac{L}{d_o}, \frac{t}{T}, c_o\right) \tag{3}$$

where $T$ is the characteristics time scale $T=(d_o/g)^{1/2}$. A correlation can be found between the initial velocity of particles and the nozzle size using orifice equation $u_o=\alpha(gd_o)^{1/2}$. Rao and Nott (2008) proposed $\alpha$=0.74 for prediction of the initial velocity of granular material. Cai et al. (2010) reported $\alpha$= 0.68 for $d_o/D_{50}$>40 and $\alpha$=0.6 for $d_o/D_{50}$<40. Similar values of $\alpha$ were employed for prediction of initial velocities of slurry jets in water (Azimi et al., 2012a, 2012b). Reynolds number Re represents the ratio of inertial to viscous forces. Effect of Re in dynamics of jet flows was found to be significant (Webster and Longmire, 2001; Azimi et al., 2012a, 2012b). Reynolds number can be formed to study oily sand jets as

$$\mathrm{Re} = \frac{u_o d_o (\rho_s - \rho_{oil})}{\mu} \tag{4}$$

Using orifice equation to express the initial sand velocity in Eq. (4) indicates a relationship between $\mathrm{Re}$ and $d_o$ as

$$\mathrm{Re} = f_3(d_o^{3/2}) \tag{5}$$

Froude number can describe the relationship between inertia and gravitational forces and it can be expressed as

$$\mathrm{Fr} = \frac{u_o}{\sqrt{gL}} = \frac{\alpha\sqrt{g d_o}}{\sqrt{gL}} \tag{6}$$

By replacing Eq. (2) into Eq. (6), Froude number can be expressed as a function of mass and nozzle diameter.

$$\mathrm{Fr} = f_4(m^{1/2}, d_o^{3/2}) \tag{7}$$

A direct correlation can be formed to describe the effects of sand mass by combining the expressions in Eqs. (5) and (7).

$$m = \frac{\pi}{4} c_o \frac{\mu^2 \rho_s}{g(\rho_s - \rho_{oil})^2} \left(\frac{\mathrm{Fr}}{\mathrm{Re}}\right)^2 \tag{8}$$

The evolution of a particle cloud can be prescribed by the buoyancy force exerted by the particle cloud (Bush et al., 2003). The initial buoyancy force for oily sand jets can be written as

$$F_B = \alpha g(\rho_s - \rho_{oil}) \left(\frac{L \pi d_o^2}{4}\right) \tag{9}$$

When sand particles exit from the nozzle, the jet's momentum increases by the imbalance

of the buoyancy and drag forces. For sand and slurry jets, the drag force dominates the flow dynamics initially and the initial momentum of sand particles transfers to the ambient water. A length scale $l_M$ can be used to show the balance between momentum and buoyancy and where the momentum dominates the jet flow (Fischer et al., 1979).

$$l_M = \frac{M^{3/4}}{B^{1/2}} \tag{10}$$

where the initial momentum and buoyancy of sand jets at the nozzle can be written as

$$M = \frac{\pi \alpha^2 g}{4} d_o^3 = f_5(d_o^3) \tag{11}$$

$$B = \frac{(\rho_s - \rho_{oil})}{\rho_{oil}} g(\frac{\pi d_o^2}{4}) u_o = f_6(d_o^{5/2}) \tag{12}$$

## 3.3 Experimental Design

Experiments were conducted in a rectangular Plexiglas tank with 0.4 m sides and 1m height. The experimental tank contains water ($\rho_w$=1000 kg/m$^3$) and a layer of canola oil ($\rho_{oil}$=920 kg/m$^3$) to form an immiscible layer with different oil thicknesses. The water depth was fixed at 0.92 m from the bottom for all experiments and the room temperature was controlled at 25ºC. Different masses of sand particles with the mean diameter of $D_{50}$=0.165 mm were dropped through a short pipe and nozzle into the tank. A Schematic diagram of the experimental setup with a cylindrical coordinate system is shown in Fig. 3-1.

Three parameters, thickness of the oil layer $h_{oil}$, nozzle diameter $d_o$, and mass of sand particles $m$ were controlled in our experiments to study the evolution of sand jets passing through oil-water interface. Six different oil layer thicknesses of 4, 6, 8, 10, 12 and 30 mm were utilized in combination with four nozzle diameters of 4, 8, 12 and 16 mm. Different masses of sand particles (i.e., $m$=5, 10, 15, 20 and 25 g) were used to represent the effects of gravitational force on the evolution of oily sand jets. Density of sand particles for $D_{50}$=0.165 mm was measured and it was $\rho_s$=2540 kg/m$^3$. Experimental details and non-dimensional parameters used in this study are summarized in Table 3-1.

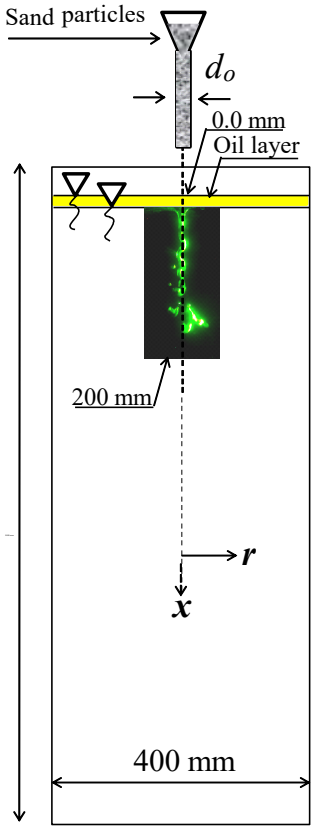


**Figure 3-1:** A schematic view of the experimental setup with a cylindrical coordinate system.

**Table 3-1:** Experimental details of oily sand jets and non-dimensional parameters.

| Test No | $h_{oil}$ ($mm$) | $d_o$ ($mm$) | $m$ ($g$) | $L/d_o$ | $h_{oil}/d_o$ | $l_M$ $\times 10^{-3}$ (m) | Re | Fr | $F_B$ ($N$) | $M$ $\times 10^{-5}$ ($m^4/s^2$) | $B$ $\times 10^{-5}$ ($m^4/s^3$) |
|---|---|---|---|---|---|---|---|---|---|---|---|
| 1 | 4 | 4 | 5 | 65.30 | 1 | 1.11 | 14.00 | 0.07 | 0.05 | 0.01 | 2.56 |
| 2 | 4 | 4 | 10 | 130.60 | 1 | 1.11 | 14.00 | 0.05 | 0.10 | 0.01 | 2.56 |
| 3 | 4 | 4 | 25 | 326.51 | 1 | 1.11 | 14.00 | 0.03 | 0.26 | 0.01 | 2.56 |
| 4 | 4 | 8 | 15 | 24.48 | 1/2 | 3.37 | 39.60 | 0.12 | 0.15 | 0.14 | 14.5 |
| 5 | 4 | 8 | 20 | 32.65 | 1/2 | 3.37 | 39.60 | 0.10 | 0.20 | 0.14 | 14.5 |
| 6 | 4 | 8 | 25 | 40.81 | 1/2 | 3.37 | 39.60 | 0.09 | 0.26 | 0.14 | 14.5 |
| 7 | 4 | 12 | 10 | 4.83 | 1/3 | 5.04 | 72.76 | 0.27 | 0.10 | 0.47 | 40.0 |
| 8 | 4 | 12 | 15 | 7.25 | 1/3 | 5.04 | 72.76 | 0.22 | 0.15 | 0.47 | 40.0 |
| 9 | 4 | 12 | 25 | 12.09 | 1/3 | 5.04 | 72.76 | 0.17 | 0.26 | 0.47 | 40.0 |
| 10 | 4 | 16 | 5 | 1.02 | 1/4 | 6.80 | 112.02 | 0.59 | 0.05 | 1.13 | 82.1 |
| 11 | 4 | 16 | 10 | 2.04 | 1/4 | 6.80 | 112.02 | 0.42 | 0.10 | 1.13 | 82.1 |
| 12 | 4 | 16 | 15 | 3.06 | 1/4 | 6.80 | 112.02 | 0.34 | 0.15 | 1.13 | 82.1 |
| 13 | 4 | 16 | 20 | 4.08 | 1/4 | 6.80 | 112.02 | 0.29 | 0.20 | 1.13 | 82.1 |
| 14 | 4 | 16 | 25 | 5.10 | 1/4 | 6.80 | 112.02 | 0.26 | 0.26 | 1.13 | 82.1 |
| 15 | 6 | 4 | 10 | 130.60 | 3/2 | 1.11 | 14.00 | 0.05 | 0.10 | 0.01 | 2.56 |
| 16 | 6 | 4 | 25 | 326.51 | 3/2 | 1.11 | 14.00 | 0.03 | 0.26 | 0.01 | 2.56 |
| 17 | 6 | 8 | 5 | 8.16 | 3/4 | 3.37 | 39.60 | 0.21 | 0.05 | 0.14 | 14.5 |
| 18 | 6 | 8 | 10 | 16.32 | 3/4 | 3.37 | 39.60 | 0.14 | 0.10 | 0.14 | 14.5 |
| 19 | 6 | 8 | 15 | 24.48 | 3/4 | 3.37 | 39.60 | 0.12 | 0.15 | 0.14 | 14.5 |
| 20 | 6 | 8 | 20 | 32.65 | 3/4 | 3.37 | 39.60 | 0.10 | 0.20 | 0.14 | 14.5 |
| 21 | 6 | 8 | 25 | 40.81 | 3/4 | 3.37 | 39.60 | 0.09 | 0.26 | 0.14 | 14.5 |
| 22 | 6 | 12 | 5 | 2.41 | 1/2 | 5.04 | 72.76 | 0.38 | 0.05 | 0.47 | 40.0 |
| 23 | 6 | 12 | 10 | 4.83 | 1/2 | 5.04 | 72.76 | 0.27 | 0.10 | 0.47 | 40.0 |
| 24 | 6 | 12 | 15 | 7.25 | 1/2 | 5.04 | 72.76 | 0.22 | 0.15 | 0.47 | 40.0 |
| 25 | 6 | 12 | 25 | 12.09 | 1/2 | 5.04 | 72.76 | 0.17 | 0.26 | 0.47 | 40.0 |
| 26 | 6 | 16 | 5 | 1.02 | 3/8 | 6.80 | 112.02 | 0.59 | 0.05 | 1.13 | 82.1 |
| 27 | 6 | 16 | 10 | 2.04 | 3/8 | 6.80 | 112.02 | 0.42 | 0.10 | 1.13 | 82.1 |
| 28 | 6 | 16 | 15 | 3.06 | 3/8 | 6.80 | 112.02 | 0.34 | 0.15 | 1.13 | 82.1 |
| 29 | 6 | 16 | 20 | 4.08 | 3/8 | 6.80 | 112.02 | 0.29 | 0.20 | 1.13 | 82.1 |
| 30 | 6 | 16 | 25 | 5.10 | 3/8 | 6.80 | 112.02 | 0.26 | 0.26 | 1.13 | 82.1 |
| 31 | 8 | 4 | 5 | 65.30 | 2 | 1.11 | 14.00 | 0.07 | 0.05 | 0.01 | 2.56 |
| 32 | 8 | 4 | 10 | 130.60 | 2 | 1.11 | 14.00 | 0.05 | 0.10 | 0.01 | 2.56 |
| 33 | 8 | 4 | 15 | 195.91 | 2 | 1.11 | 14.00 | 0.04 | 0.15 | 0.01 | 2.56 |
| 34 | 8 | 8 | 5 | 8.16 | 1 | 3.37 | 39.60 | 0.21 | 0.05 | 0.14 | 14.5 |
| 35 | 8 | 8 | 20 | 32.65 | 1 | 3.37 | 39.60 | 0.10 | 0.20 | 0.14 | 14.5 |
| 36 | 8 | 8 | 25 | 40.81 | 1 | 3.37 | 39.60 | 0.09 | 0.26 | 0.14 | 14.5 |
| 37 | 8 | 12 | 5 | 2.41 | 2/3 | 5.04 | 72.76 | 0.38 | 0.05 | 0.47 | 40.0 |
| 38 | 8 | 12 | 10 | 4.83 | 2/3 | 5.04 | 72.76 | 0.27 | 0.10 | 0.47 | 40.0 |

| | | | | | | | | | | | |
|---|---|---|---|---|---|---|---|---|---|---|---|
| 39 | 8 | 12 | 25 | 12.09 | 2/3 | 5.04 | 72.76 | 0.17 | 0.26 | 0.47 | 40.0 |
| 40 | 10 | 4 | 5 | 65.30 | 5/2 | 1.11 | 14.00 | 0.07 | 0.05 | 0.01 | 2.56 |
| 41 | 10 | 4 | 15 | 195.91 | 5/2 | 1.11 | 14.00 | 0.04 | 0.15 | 0.01 | 2.56 |
| 42 | 10 | 8 | 10 | 16.32 | 5/4 | 3.37 | 39.60 | 0.14 | 0.10 | 0.14 | 14.5 |
| 43 | 10 | 8 | 25 | 40.81 | 5/4 | 3.37 | 39.60 | 0.09 | 0.26 | 0.14 | 14.5 |
| 44 | 10 | 12 | 5 | 2.41 | 5/6 | 5.04 | 72.76 | 0.38 | 0.05 | 0.47 | 40.0 |
| 45 | 10 | 12 | 10 | 4.83 | 5/6 | 5.04 | 72.76 | 0.27 | 0.10 | 0.47 | 40.0 |
| 46 | 10 | 12 | 25 | 12.09 | 5/6 | 5.04 | 72.76 | 0.17 | 0.26 | 0.47 | 40.0 |
| 47 | 10 | 16 | 5 | 1.02 | 5/8 | 6.80 | 112.02 | 0.59 | 0.05 | 1.13 | 82.1 |
| 48 | 10 | 16 | 10 | 2.04 | 5/8 | 6.80 | 112.02 | 0.42 | 0.10 | 1.13 | 82.1 |
| 49 | 10 | 16 | 15 | 3.06 | 5/8 | 6.80 | 112.02 | 0.34 | 0.15 | 1.13 | 82.1 |
| 50 | 10 | 16 | 20 | 4.08 | 5/8 | 6.80 | 112.02 | 0.29 | 0.20 | 1.13 | 82.1 |
| 51 | 10 | 16 | 25 | 5.10 | 5/8 | 6.80 | 112.02 | 0.26 | 0.26 | 1.13 | 82.1 |
| 52 | 12 | 8 | 5 | 8.16 | 3/2 | 3.37 | 39.60 | 0.21 | 0.05 | 0.14 | 14.5 |
| 53 | 12 | 8 | 10 | 16.32 | 3/2 | 3.37 | 39.60 | 0.14 | 0.10 | 0.14 | 14.5 |
| 54 | 12 | 8 | 25 | 40.81 | 3/2 | 3.37 | 39.60 | 0.09 | 0.26 | 0.14 | 14.5 |
| 55 | 12 | 12 | 5 | 2.41 | 1 | 5.04 | 72.76 | 0.38 | 0.05 | 0.47 | 40.0 |
| 56 | 12 | 12 | 10 | 4.83 | 1 | 5.04 | 72.76 | 0.27 | 0.10 | 0.47 | 40.0 |
| 57 | 12 | 12 | 25 | 12.09 | 1 | 5.04 | 72.76 | 0.17 | 0.26 | 0.47 | 40.0 |
| 58 | 12 | 16 | 5 | 1.02 | 3/4 | 6.80 | 112.02 | 0.59 | 0.05 | 1.13 | 82.1 |
| 59 | 12 | 16 | 10 | 2.04 | 3/4 | 6.80 | 112.02 | 0.42 | 0.10 | 1.13 | 82.1 |
| 60 | 12 | 16 | 15 | 3.06 | 3/4 | 6.80 | 112.02 | 0.34 | 0.15 | 1.13 | 82.1 |
| 61 | 12 | 16 | 20 | 4.08 | 3/4 | 6.80 | 112.02 | 0.29 | 0.20 | 1.13 | 82.1 |
| 62 | 12 | 16 | 25 | 5.10 | 3/4 | 6.80 | 112.02 | 0.26 | 0.26 | 1.13 | 82.1 |
| 63 | 30 | 8 | 5 | 8.16 | 15/4 | 3.37 | 39.60 | 0.21 | 0.05 | 0.14 | 14.5 |
| 64 | 30 | 8 | 10 | 16.32 | 15/4 | 3.37 | 39.60 | 0.14 | 0.10 | 0.14 | 14.5 |
| 65 | 30 | 8 | 15 | 24.48 | 15/4 | 3.37 | 39.60 | 0.12 | 0.15 | 0.14 | 14.5 |
| 66 | 30 | 8 | 25 | 40.81 | 15/4 | 3.37 | 39.60 | 0.09 | 0.26 | 0.14 | 14.5 |
| 67 | 30 | 12 | 5 | 2.41 | 5/2 | 5.04 | 72.76 | 0.38 | 0.05 | 0.47 | 40.0 |
| 68 | 30 | 12 | 10 | 4.83 | 5/2 | 5.04 | 72.76 | 0.27 | 0.10 | 0.47 | 40.0 |
| 69 | 30 | 12 | 15 | 7.25 | 5/2 | 5.04 | 72.76 | 0.22 | 0.15 | 0.47 | 40.0 |
| 70 | 30 | 12 | 25 | 12.09 | 5/2 | 5.04 | 72.76 | 0.17 | 0.26 | 0.47 | 40.0 |
| 71 | 30 | 16 | 5 | 1.02 | 15/8 | 6.80 | 112.02 | 0.59 | 0.05 | 1.13 | 82.1 |
| 72 | 30 | 16 | 10 | 2.04 | 15/8 | 6.80 | 112.02 | 0.42 | 0.10 | 1.13 | 82.1 |
| 73 | 30 | 16 | 15 | 3.06 | 15/8 | 6.80 | 112.02 | 0.34 | 0.15 | 1.13 | 82.1 |
| 74 | 30 | 16 | 25 | 5.10 | 15/8 | 6.80 | 112.02 | 0.26 | 0.26 | 1.13 | 82.1 |

A sliding plate was used to control the release of sand particles without disturbing the sand jets and oil surface. The release height was kept at the most 8 mm above the oil surface to minimize the excess initial momentum of the jet due to release height. Sand particles were released by removing the plate from the bottom of the nozzle.

A minimum relaxation time of 4 minutes was allowed between each experiment to stabilize the oil-water interface. The relaxation time helped to remove all oil and water droplets from previous experiments and prevent any historical impact on a new jet. A small amount of oil was dragged by sand particles during the experiments. Mixture of oil and sand particles were deposited at the bottom of the tank after each test. The thickness of oil layer was measured after each test and a suitable volume of oil was added to keep the interface to its original position. The background water in the tank was illuminated using a continuous laser sheet as a light source with a wave length of 532 nm (Laserwave, G2000). The evolution of sand jets passing through oil-water interface was recorded with a high speed camera (Photron-Fastcam 1024PCI-100KC) with a resolution of 1024×1024 pixels. Raw images were recorded with the speed of 60 frames per second and they were controlled by computer grabber software (Photron Motion Tools). The area of interest was a rectangle of 0.40 m×0.324 m and the area of interest was located 0.011 m below the water surface. Frontal width and velocity of sand jets were measured accurately using an image processing technique. For each experiment, a distance $x$ between the front of oily sand jet and the nozzle was measured and measurements were fitted by a polynomial equation for each test. Frontal velocity at each time step was calculated using the derivative of the fitted polynomial equation for $x$.

## 3.4 Experimental Results

### *3.4.1- Evolution of Sand Jets Passing Through an Oil Layer*

Fig. 3-2 shows the snapshot images of sand jets with different initial parameters at different times.

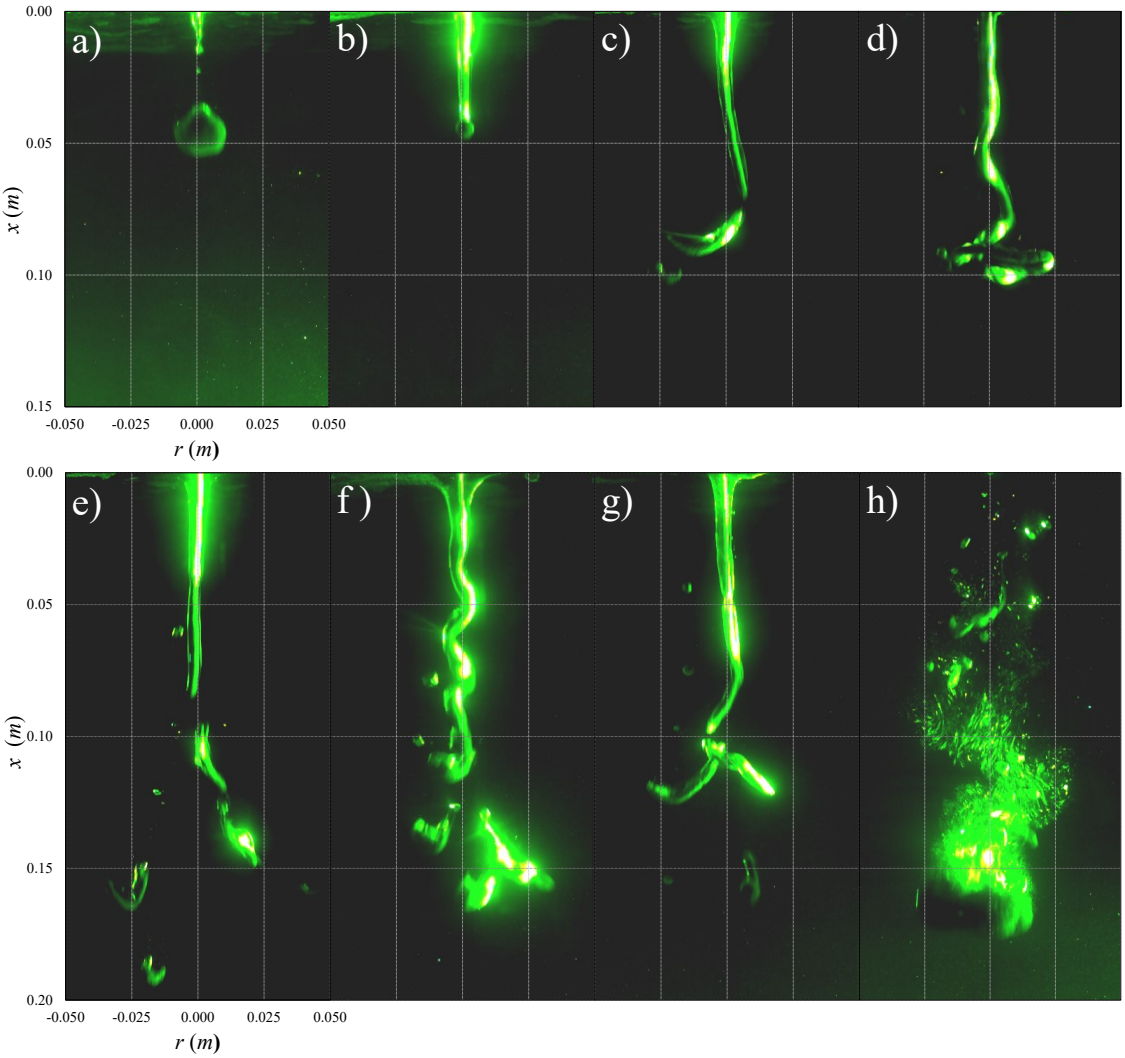


**Figure 3-2:** Snapshot images of sand jets passing through an oil-water interface at different times with different initial parameters. a) Ball shape [$h_{oil}$=6 mm, $d_o$=16 mm, $m$=5g, $t$=0.233 s]; b) Bar shape [$h_{oil}$=6 mm, $d_o$=4 mm, $m$=10g, $t$=0.317 s]; c) Hook shape [$h_{oil}$=10 mm, $d_o$=4 mm, $m$=15g, $t$=0.683 s]; d) Torsion [$h_{oil}$=4 mm, $d_o$=8 mm, $m$=25g, $t$=0.666 s]; e) Separation [$h_{oil}$=10 mm, $d_o$=4 mm, $m$=15g, $t$=1.183 s]; f) Trialing wave

[$h_{oil}$=12 mm, $d_o$=8 mm, $m$=10g, $t$=0.683 s]; g) Bifurcation [$h_{oil}$=8 mm, $d_o$=4 mm, $m$=10g, $t$=1.0 s]; h) Bursting [$h_{oil}$=12 mm, $d_o$=16 mm, $m$=20g, $t$=0.716 s].

Eight different shapes of sand jets were observed in this study. Four distinct shapes were found for the smallest nozzle diameter ($d_o$=4 mm) as a bar shape at the beginning of the experiment ($0<t<0.4$ s), hook shape at the middle ($t<0.7$ s) and separation or bifurcation of sand jets at the end of experiments ($0.6<t<1.0$ s) (see Figs. 3-2b, 3-2c, 3-2e and 3-2g). The bar shape forms at the beginning of the jet stream for $d_o$=4 mm (i.e., Re=14 and $0.03<$Fr$<0.07$), $h_{oil}<30$mm and $m\leq25$ g (see Fig. 3-2b). Formation of bar shape is consistent with observations of Nicolas (2002) on stable jets using acrylic resin particles and silicone oil. No bursting was observed for this range of Reynolds number. Oily sand jets formed a hook shape for $0.4<t<0.7$ s (see Fig. 3-2c).

Oily sand jets were classified into stable and unstable jets. Stable jets were observed for oily sand jets passing through the smallest nozzle diameter ($d_o$=4 mm), and $h_{oil}<30$mm. It was found that the mass of sand particles was not able to destabilize oily sand jets. Images of stable oily sand jets are shown in Figs. 3-2b, 3-2c, 3-2e, and 3-2g. Jet splitting and bursting were observed in unstable oily sand jets (see Figs. 3-2d, 3-2f and 3-2h). Unstable jets were found for larger nozzle sizes (8 mm$\leq d_o\leq$16 mm). Two different shapes were observed for unstable sand jets. The unstable trailing wave occurred for $h_{oil}<30$ mm, $d_o$=8, 12 mm, $m>5$g (Fig. 3-2f). The unstable trailing wave formed a torsion head at front for higher masses of sand particle $m>10$g (Fig. 3-2d). Formation of the torsion head can be related to Reynolds number. Reynolds number for trailing wave and torsion head were Re=39.60 and 72.76, respectively.

Two distinct regimes were observed for the largest nozzle size in this study ($d_o$=16 mm). In all cases, a group of particles covered with a thin oil layer entered into the ambient water. The frontal head separated from the tail as soon as they come into the ambient water and developed two different shapes based on the oil layer thickness and mass (see Figs. 3-2a and 3-2h). Sand jets with small masses ($m$<15 g), thick oil layers ($h_{oil}$>8mm) and high Froude numbers (Fr>0.34) formed a ball shape (Fig. 3-2a) while, other sand jets with higher mass ($m$>15 g) and small Froude numbers (Fr<0.34), suddenly burst into small particles (Fig. 3-2h). For narrow oil layers ($h_{oil}\leq$ 8mm) bursting of sand cloud occurred for the entire ranges of particle masses. Our preliminary observations indicate that the initial momentum of sand particles can significantly changes the evolution of oily sand jets in water. Therefore, effects of initial momentum were studied by changing the mass of oily sand jets. Two different groups of oily sand jets with initial sand masses of $m$=10 and 25 g were investigated in detail. Frontal widths and velocities of oily sand jets with small mass ($m$=10 g) and large mass ($m$=25 g) of particles were studied in detail and results were shown in sections 3.4.2 and 3.4.3.

### *3.4.2- Frontal Width*

Effects of initial parameters on the growth of frontal widths of oily sand jets are studied in this section. Fig. 3-3 demonstrates the variations of sand jets frontal widths along the axis of the jets. The error bars indicate a maximum measurement uncertainty of 7.7% for $d_o$=4 mm.

The frontal width $w_f$ and the distance from the nozzle $x$ are normalized by the nozzle diameter $d_o$. Frontal width for four nozzle size (i.e., $d_o$=4, 8, 12, 16 mm), $h_{oil}$=6, 12 and 30 mm and two different mass (i.e., $m$= 10 and 25 g) are shown in Fig. 3-3. The growth

rate of water jets with a spreading rate of 0.25 (Turner, 1969) and the growth rate of thermal of heavy salt with a spreading rate of 0.375 (Lee and Chu, 2003) were added in this figure for comparison. Fig. 3-3a, shows the frontal width for all nozzle diameters, $h_{oil}$=6 mm and $m$=10 g. This figure shows that for $d_o$>4 mm, frontal widths increased linearly with $x/d_o$ and the growth rates were similar to the single-phase buoyant thermal. As can be seen in Fig. 3-3a, the growth rate of oily sand jets for small nozzle size ($d_o$=4 mm) is smaller than the growth rate of single-phase water jet for $x/d_o \leq 30$. For $x/d_o$>30, instability of oily sand jets enhanced the spreading and the growth rate becomes similar to the single-phase water jets.

Oily sand jets became more stable when they passed through thicker oil layers. Fig. 3-3b shows the variations of the frontal width of oily sand jets for $m$=10 g and $h_{oil}$=12 mm. This figure indicates that the growth rate is independent of the nozzle size. As can be seen, oily sand jets did not spread for $x/d_o \leq 10$ and they formed a bar shape (Fig. 3-2b). Instability began for $x/d_o$>10 and it caused intense spreading of oily sand jets with a spreading rate of 0.4. At this stage, oily sand jets changed from a bar shape to a torsion shape (see Fig. 3-2d).

Fig. 3-3c shows the growth of the frontal widths for $m$=10 g and $h_{oil}$=30 mm. Bar shape was observed for oily sand jets with $h_{oil}$=30 mm similar to oily sand jets with $h_{oil}$=12 mm. Figs. 3-3d-3-3f show the effects of oil layer thickness and nozzle size on oily sand jets with $m$=25 g. Fig. 3-3d shows the spreading of oily sand jets passing through a thin layer of oil ($h_{oil}$=6 mm). Bar shape was formed for $x/d_o$<10 then, the frontal width increased significantly due to intense instability and a torsion shape was formed at the front of oily sand jets for $10 \leq x/d_o \leq 30$ (see Fig. 3-2d).

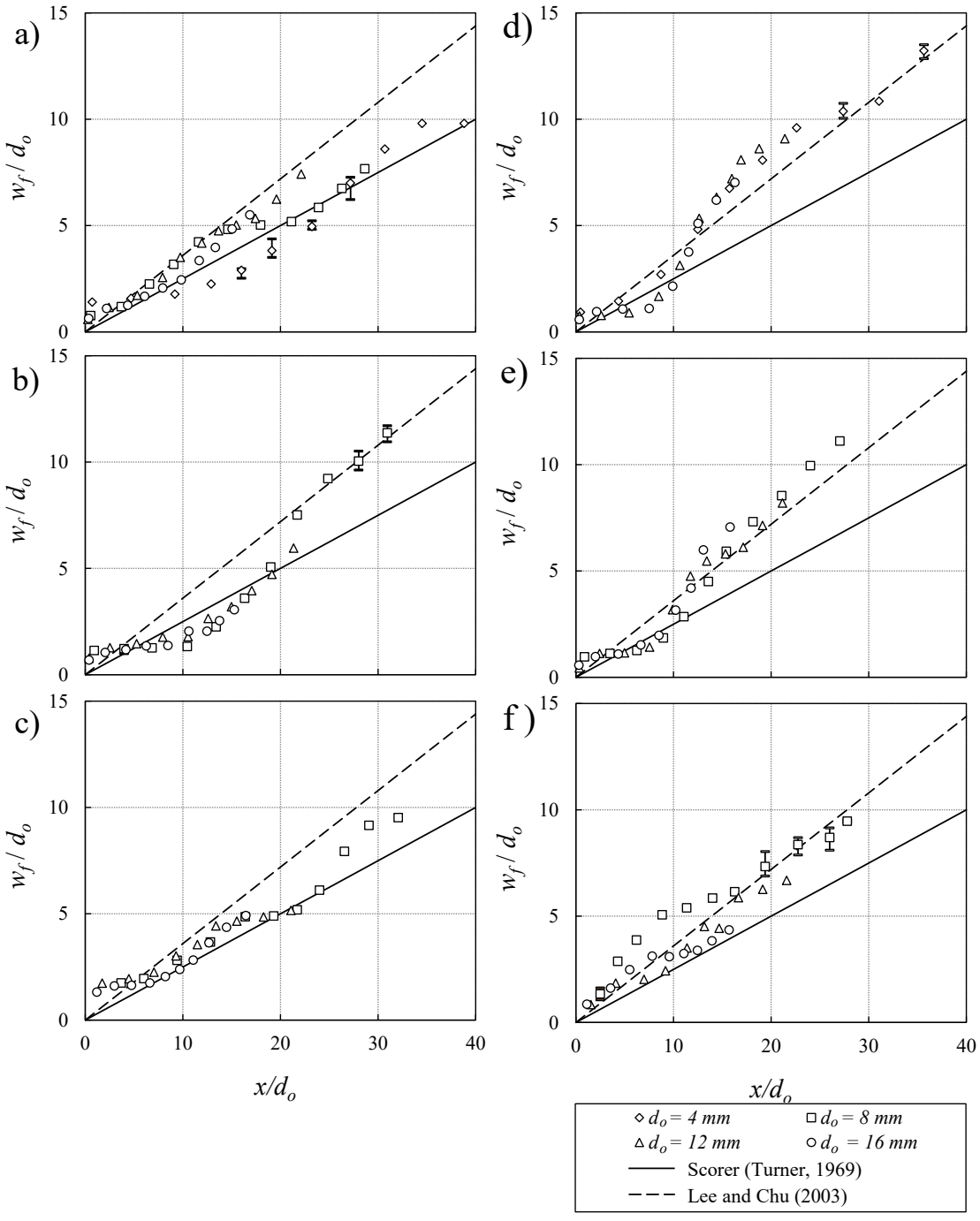


**Figure 3-3:** Variations of the normalized width of sand jets $w_f/d_o$ passing through an oil layer with the normalized distance $x/d_o$ for different sand masses, oil layer thicknesses and nozzle diameters; a) $m$=10 g, $h_{oil}$=6 mm; b) $m$=10 g, $h_{oil}$=12 mm; c) $m$=10 g, $h_{oil}$=30 mm; d) $m$=25 g, $h_{oil}$=6 mm; e) $m$=25 g, $h_{oil}$=12 mm; f) $m$=25 g, $h_{oil}$=30 mm.

For $x/d_o$>30, the growth rate of oily sand jets was similar to the single-phase buoyant thermal. Bar shape was also observed for $h_{oil}$=12 mm (see Fig. 3-3e) for $x/d_o$<10. Our observation indicated that thicker oil layer damped the instability generated by the difference on the surface tension of both layers. On the other hand, excess momentum due to higher mass of sand particles augments the jet instability and causes higher frontal width due to formation of a torsion shape.

Excess momentum due to higher sand mass in oily sand jets with $m$=25 g was balanced with the damping effect of higher oil thickness ($h_{oil}$=12 mm). This resulted in a linear growth rate of the frontal width similar to the growth rate of a single-phase buoyant thermal. More damping was observed for $h_{oil}$=30 mm except for oily sand jets with $d_o$=8 mm. As can be seen in Fig. 3-3f, the growth rate of oily sand jets in this regime was similar to a single-phase buoyant thermal. Separation of groups of particles covered with a thin layer of oil caused abnormal frontal widths for $d_o$=8 mm and for 5<$x/d_o$<20. The growth rate of this test for $x/d_o$>20 was also similar to the prediction of Lee and Chu (2003) for a single-phase buoyant thermal.

### *3.4.3- Frontal Velocity*

Variations of the frontal velocity of oily sand jets with non-dimensional time $t/T$ for different nozzle sizes, oil layer thicknesses and for $m$=10 g and 25 g are shown in Fig. 3-4. Figs. 3-4a and 3-4c show the variations of the frontal velocity for small mass of particles ($m$=10 g) and Figs. 3-4d and 3-4f show the effects of nozzle diameter and oil thicknesses for large mass of particles ($m$=25 g). Fig. 3-4a shows the effect of oil layer thickness on correlations of the normalized frontal velocity with time for small nozzle size ($d_o$=4 mm). Jet flow acceleration was observed for all oil layer thicknesses and the

peak frontal velocities occurred at $t/T$=3~6. Frontal velocities in this range increase by 20%−40% of the initial jet velocities. The acceleration of frontal head at the beginning of experiments may be due to formation of a bar shape in this time range. Similar velocity accelerations were found in other tests with different nozzle sizes and oil layer thicknesses indicated the existence of a bar shape in those experiments.

Sharp deceleration was observed once oily sand jets passed the peak velocity. The deceleration phase occurred for $3<t/T<16$. At this stage, frontal velocities decreased linearly with time. This phenomenon resulted from accumulation of sand particles at oil-water interface and changing the initial bar or ball shapes of the oily sand jet to either a hook or a torsion shape. This may cause the frontal velocity to be even smaller than the initial velocity (see Fig. 3-4a). A minimum velocity of $u_f/u_o$=0.75 that observed for $h_{oil}$=4mm was due to formation of a hook shape in this test. The contact surface of sand particles covered with a thin oil layer increased once the hook shape initiated. This resulted in higher flow resistance and deceleration of oily sand jet front.

Second acceleration phase with different acceleration rates can be developed after the deceleration phase. At this stage, the hook or torsion shapes reached their maximum sizes and they dropped directly to the bottom of the tank. This phenomenon caused an increase in frontal velocity. Second deceleration phase in Fig. 3-4a occurred for $t/T$>22. Deceleration may be due to separation of oily sand jets into groups of sand particles and deviation of oily sand jets from vertical path (see Fig. 3-2e). A gradual increase of frontal velocity for $h_{oil}$=6mm was also due to separation of oily sand jets. At this stage, the separated group of particles fall directly as a ball (see Fig. 3-4a).

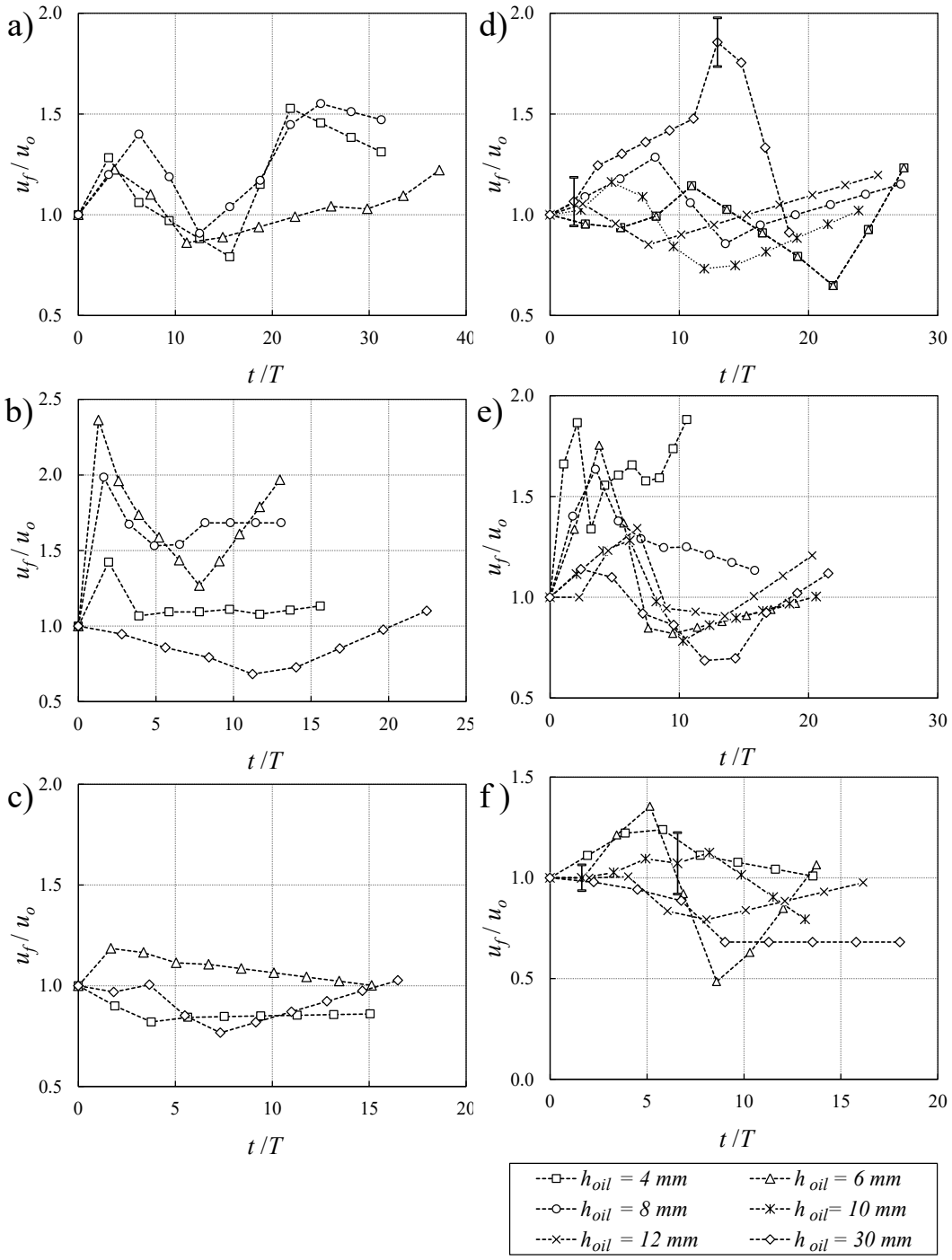


**Figure 3-4:** Effects of sand mass, oil layer thickness and nozzle size on the frontal velocity of sand with time. a) $m$=10 g, $d_o$=4 mm; b) $m$=10g, $d_o$=12 mm; c) $m$=10g, $d_o$=16 mm; d) $m$=25 g, $d_o$=8 mm; e) $m$=25g, $d_o$=12 mm; f) $m$=25g, $d_o$=16 mm.

Frontal velocity patterns of oily sand jets with $d_o$=12 mm were similar to $d_o$=4 mm except the peak velocity of the first acceleration phase occurred earlier at $t/T$=2. Similar to smaller nozzle size, deceleration phase occurred due to formation of hook and torsion. Once the hook or torsion reached their maximum sizes, the frontal velocity of oily sand jets reached the plateau unless bursting phenomenon happens. Different velocity patterns were observed for the thickest oil layer ($h_{oil}$=30 mm). A large ball with a tail was formed in this test and it descends following a sinusoidal pattern. This caused a slight deceleration on the vertical component of the frontal velocity of the oily sand jet. The sinusoidal flow of sand ball damped and the ball fell directly for $t/T$>11. At this stage, many trapped bubbles escaped from the ball and this resulted in a slight increase on frontal velocity due to buoyancy reduction.

Different flow patterns were observed for larger nozzles ($d_o$=16 mm). Fig. 3-4c shows the variations of frontal velocities of oily sand jets with different oil layers. This figure shows the same trend for all oil layer thickness and it is almost constant after $t/T$>5. Figs. 3-4d and 3-4f show the variations of oily sand jet front for larger mass ($m$=25 g). Similar to jets with smaller mass, variations of the frontal velocity can be linked to the shapes of the oily sand jets. Uncertainties on frontal velocities of oily sand jets were shown in Fig. 3-4d for $h_{oil}$=30 mm and Fig. 3-4f for $h_{oil}$=10 mm. The maximum variations of the frontal velocity in Figs. 3-4d and 3-4f were ±11.1% and ±14.1%, respectively.

### *3.4.4-Particle Separation (Bursting)*

Detail observations on variations of frontal widths and velocities indicated that bursting of oily sand jets can significantly alter the dynamics and mixing of particles in the ambient. Three different bursting mechanisms were observed. Fig. 3-5 shows the images

of those bursting mechanisms named as bifurcation bursting, rear bursting and multiple bursting. Fig. 3-5a shows an image of bifurcation bursting.

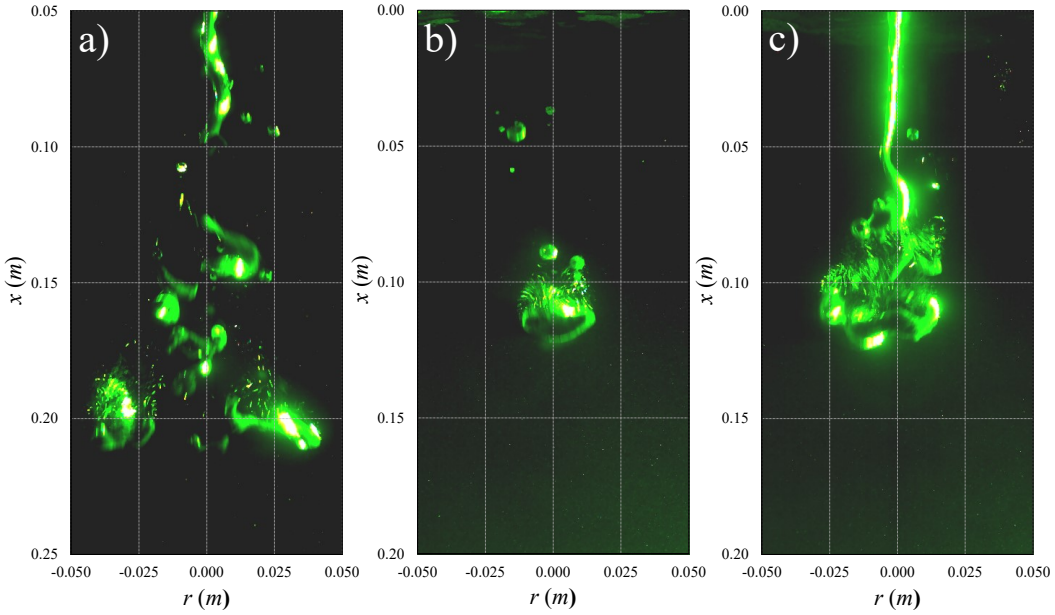


**Figure 3-5:** Dissimilarity in bursting type under the influence of oil layer, nozzle diameter and particle mass. a) Bifurcation bursting [Test No. 5, $h_{oil}$=4 mm, $d_o$=8 mm, $m$=20g, $L/d_o$=32.6]; b) Rear bursting [Test No. 10, $h_{oil}$= 4 mm, $d_o$=16 mm, $m$=5g, $L/d_o$=1]; c) Multiple [Test No. 23, $h_{oil}$=6 mm, $d_o$=12 mm, $m$=10g, $L/d_o$=4.83].

Using Eq. (2) to convert particle mass to a length scale $L$, it can clearly showed that the bifurcation bursting occurred for large $L/d_o$ (i.e., Test No. 5, $L/d_o$=32.6). This type of bursting occurs long after the commencement of oily sand jets at $t/T$≈20. In most cases, oily sand jets formed a torsion front (see Fig. 3-2d). Then, due to separation of trapped air bubble from the head, the torsion front distorted into a bifurcation front (see Fig. 3-2g). The bifurcation front lost the thin oil cover due to skin friction drag force exerted by ambient water and bursting occurred. After bursting, the frontal velocity decreased and the front width increased.

The second type of bursting occurred when small masses of particles passed through a large nozzle. Fig. 3-5b shows the image of particle cloud formed in test No. 10 with $L/d_o$=1. A ball was formed from the onset of particle motion and as it descended, the thin oil layer thickness covering sand particles became thinner. The thin oil layer ruptured once the trapped air bubbles escaped from the ball (Fig. 3-5b). Flow of air bubble caused instability at the rear of the ball and rear busting occurred. The rear bursting can be easily detected by sudden deceleration of the frontal velocity (see Fig. 3-4c, $h_{oil}$=30 mm). Multiple bursting formed relatively earlier than bifurcation bursting. Fig. 5c shows an image of multiple bursting for test No. 23 with the $L/d_o$ of 4.83. In this case, masses of particles are large enough to form a frontal head (i.e., torsion head) but bursting occurs once air bubbles escape from number of locations at the front. This caused multiple oil layer rupture and bursting at different parts of the oily sand jet.

Since dynamics of oily sand jets such as frontal width and velocity are related to bursting, it is important to estimate when bursting occurs. Study different types of bursting revealed the fact that bursting mechanisms correlated with the $L/d_o$. In this regard, bursting time at each test was recorded and normalized data were plotted against $L/d_o$. Fig. 3-6 shows the variations of the normalized bursting time $t/T$ with $L/d_o$ for three different oil layer thicknesses.

Uncertainties on detecting bursting time were shown in Fig. 3-6b for $h_{oil}$=6 mm and $d_o$=8, 12 mm. The maximum variations of bursting time were ±10% and ±4.2% for $d_o$=8, 12mm, respectively.

An adverse relationship was found between the normalized bursting time and nozzle diameter. Fig. 3-6a shows the variations of $L/d_o$ with $t/T$ for $h_{oil}$=4 mm. As can be seen,

this correlation can be clearly described by a linear equation. No bursting occurred for $d_o$=4mm, since the frontal part splits into many small groups of particles. Those groups of particles were not large enough to generate large shear force around the thin oil layer and cause bursting.

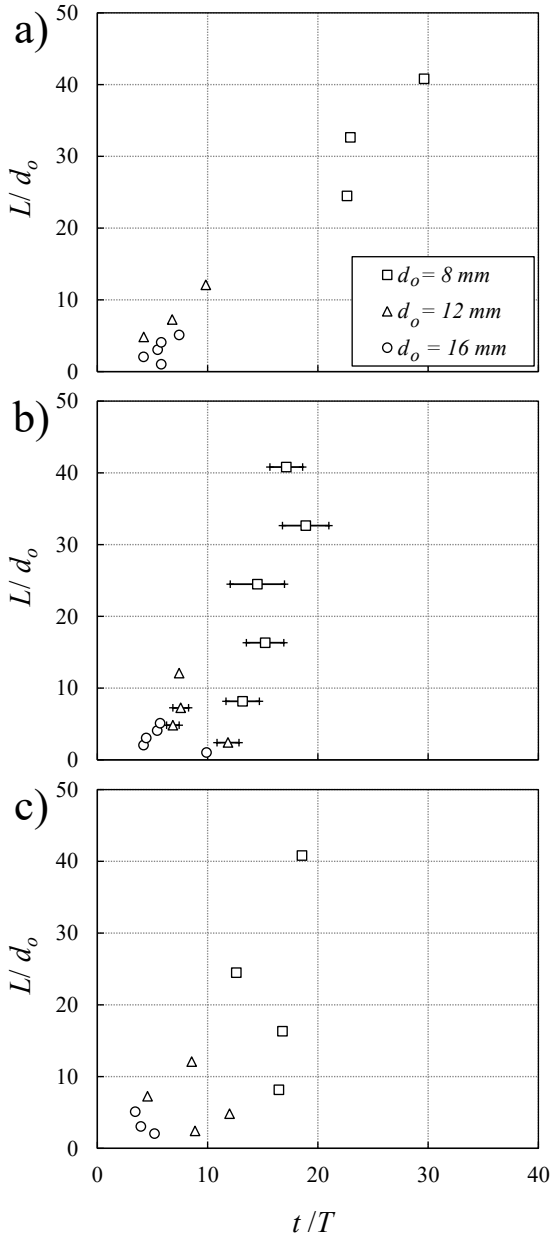


**Figure 3-6:** Effect of nozzle size on the correlation between the normalized mass $L/d_o$ and the normalized time $t/T$ for a) $h_{oil}$=4 mm; b) $h_{oil}$=6 mm; c) $h_{oil}$=30 mm.

Fig. 3-6c shows the effect of $L/d_o$ on bursting time for the thickest oil layer. As can be seen in this figure, nozzle diameter had significant effect on bursting time and bursting time decreased as nozzle diameter increased whereas $L/d_o$ ratio had trivial impact on bursting time for oily sand jets passing through a thick oil layer (i.e., $h_{oil}$=30 mm).

### *3.4.5-Shear Stress*

Sand particles encapsulate when passing though oil layer and form a semi-cylindrical shape with a diameter of $d_o$. Newton second law can be applied to equate force imbalances with the rate of change of momentum. The forces exerted on the encapsulated sand particles with a velocity $u_f$, density of $\rho_m = c_o\rho_s$ and sand concentration of $c_o$, are the gravitational force $F_g$, form drag force $F_D$, and skin friction drag force $F_\tau$ due to the friction between oil layer and encapsulated sand particles. The Newton second law for a group of particles can be written as:

$$\rho_s c_o Q(u_o - u_f) = \Sigma F = F_g - F_D - F_\tau \tag{13}$$

Where $Q=(\pi A^2/4)u_o$ is the volume flux of sand particles. Gravitational, force and skin friction drag forces can be written as

$$F_g = \frac{\pi A^2}{4} x c_o \rho_s g \tag{14}$$

$$F_D = \frac{\pi A^2}{4} x \rho_w g \tag{15}$$

$$F_\tau = \pi A x \tau \tag{16}$$

where $A$ is the projected area of oily sand jets and $\tau$ is the shear stress. Investigation on variations of bursting time with different nozzle diameter indicates that the shear stress of

oily sand jets can be related to the initial parameters. The skin friction force was calculated using momentum equation (Eq. (13)) and shear stresses were estimated from Eq. (16). Fig. 3-7a shows the effects of nozzle size on variations of shear stress with $x/d_o$ for $h_{oil}$>4 mm and $m$=10 g. The estimated shear stresses were varied from 7 to 22 Pa. Similar variations were observed for larger masses of oily sand jets.

As can be seen, nozzle diameter has a direct relationship with shear stress and the magnitude of the shear stress is independent of $x/d_o$. Orifice equation shows a direct relationship between the initial velocity of the jet and nozzle size as $u_o \sim d_o^{1/2}$. This explains that oily sand jets with higher nozzle size have higher initial momentum which results in generation of higher shear stress.

A thin layer of oil can be formed for oil sand jets passing through larger nozzle. For those cases the thin oil layer experienced higher shear stress and it ruptured faster. This can be clearly seen in Fig. 3-6 that the bursting occurs relatively faster in oily sand jets with larger nozzle diameters. As can be seen from Fig. 3-7a, shear stress was also independent of oil layer thickness and it slightly reduced for $h_{oil}$=30 mm. In order to eliminate the effects of nozzle diameter on the shear stress, $\tau$ was normalized with the initial velocity and variations of the normalized shear stress with $x/d_o$ were plotted in Fig. 3-7b. As can be seen the normalized shear stress was constant for all tests with a value of 0.16±0.01. The magnitude of the normalized shear stress can be related to the property of canola oil.

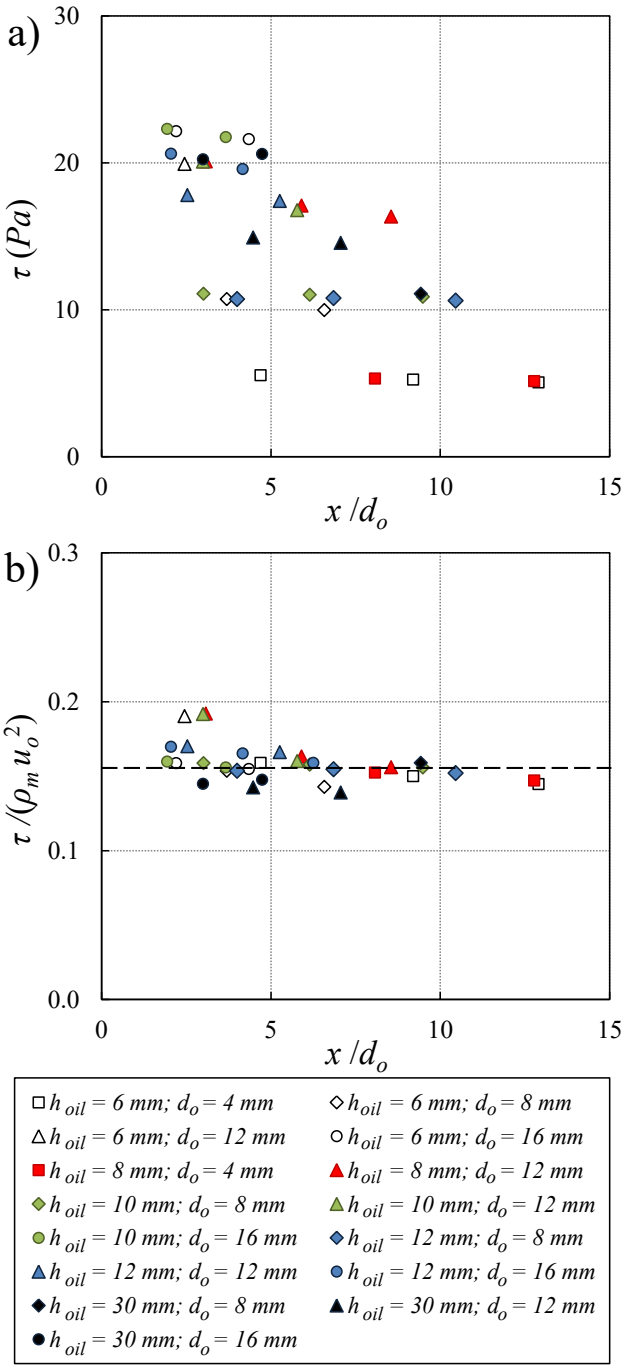


**Figure 3-7:** Variations of the average shear stress of an oil-water interface $\tau$ along the axis of the jet for $m$=10 g.

### *3.4.6- Trailing of Sand Jets*

Instability waves were observed in the trailing part of oily sand jets for $m$>5 g. Figure 3-8 shows the development of a sinusoidal instability wave for $m$=25 g. Instability of the trailing section caused a slight wobbling of the frontal head which magnifies the amplitude of the waves until it separated from the head. A typical example of this behaviour is shown in Fig. 3-8 for test No. 36 ($h_{oil}$=8 mm, $d_o$=8 mm, $m$=25g).

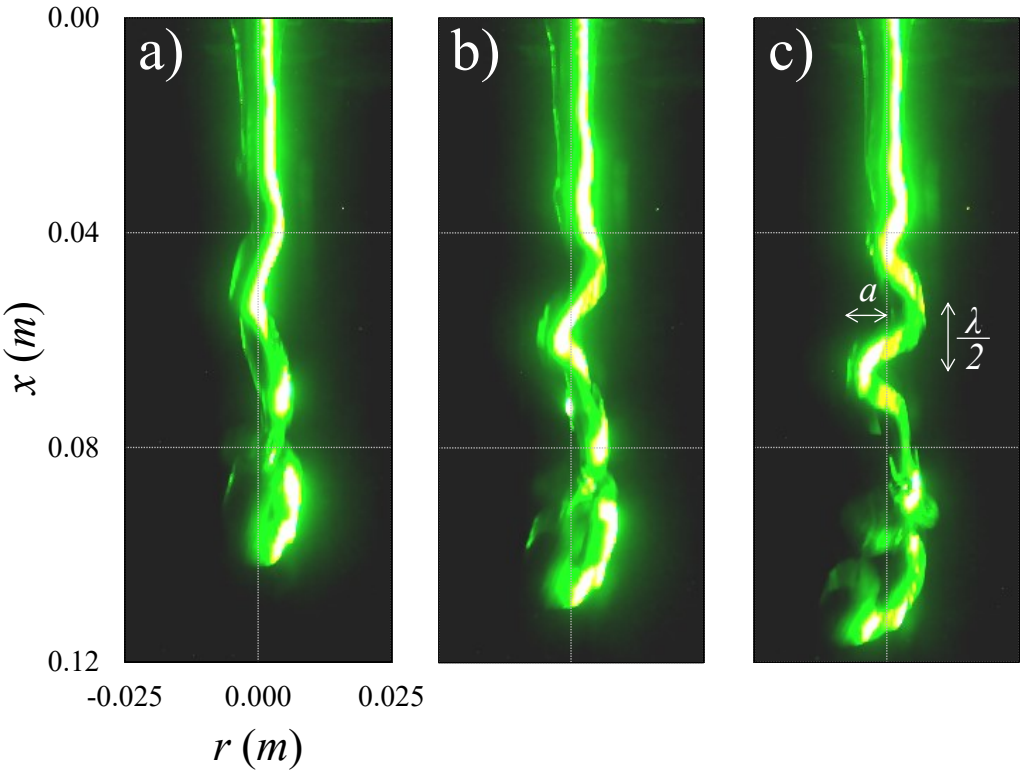


**Figure 3-8:** The evolution of compression in the trailing of sand jets' head passing through an oil layer for test No. 36 ($h_{oil}$=8 mm, $d_o$=8 mm, $m$=25g) at different times. a) $t$=0.4 s; b) $t$=0.433 s; c) $t$=0.466 s.

Images (3-8a-3-8c) were taken 0.4 s, 0.433 s, 0.466 s after the beginning of the test, respectively. Since instability of the trailing section can be correlated with other characteristics of the jets such as frontal velocity and width, it is important to estimate

how sinusoidal instability generates, grows and decays. This can be studied by analysing the variations of the amplitude $a$ and the wavelength $\lambda$ of trailing waves at different times and for different cases. Our observations indicated that the nozzle diameter have significant impacts on the evolution of oily sand jets. Therefore, wave characteristics were normalized with $d_o$ to eliminate scaling effects.

Figs. 3-9 and 3-10 show the variations of the normalized wave formation, $\lambda/d_o$ and $a/d_o$ time $t/T$ for four different oil layer thicknesses, respectively. Uncertainties of measurements for wavelength were shown in Figs 3-9a, 3-9c and 3-9d. The maximum variations of wavelengths were ±9.1% for $d_o$=4mm and $m$=25 g (see Fig. 3-9a). Figs. 3-10a, 3-10c and 3-10d show the uncertainties of wave amplitude for $d_o$=4, 8 mm and $m$=25, 10,15 g, respectively. The maximum variations of wave amplitude were ±12.5% and ±16.6% for Figs. 10a and 10c. An inverse relationship was found between the normalized wave formation time and nozzle diameter. This can be clearly seen for tests with thin oil layer (Fig. 3-9a). In this figure, trailing waves formed at $t/T$≈30 for jets with $d_o$=4 mm whereas the normalized wave time for $d_o$=12 mm was around 5. Depends on variations of $a$ and $\lambda$ with time four possible behaviour can be explained. Trailing waves can grow or decay if both $a$ and $\lambda$ increase or decrease. Wave distortion can be occurred if either $a$ or $\lambda$ increases. Sudden increase of wave amplitude or wavelength reduction shows that the trailing wave compresses. In contrary, sudden reduction of $a$ or growth of $\lambda$ indicates wave stretching. Therefore, in order to understand the dynamics of trailing waves, Figs. 3-9 and 3-10 should be interpreted simultaneously.

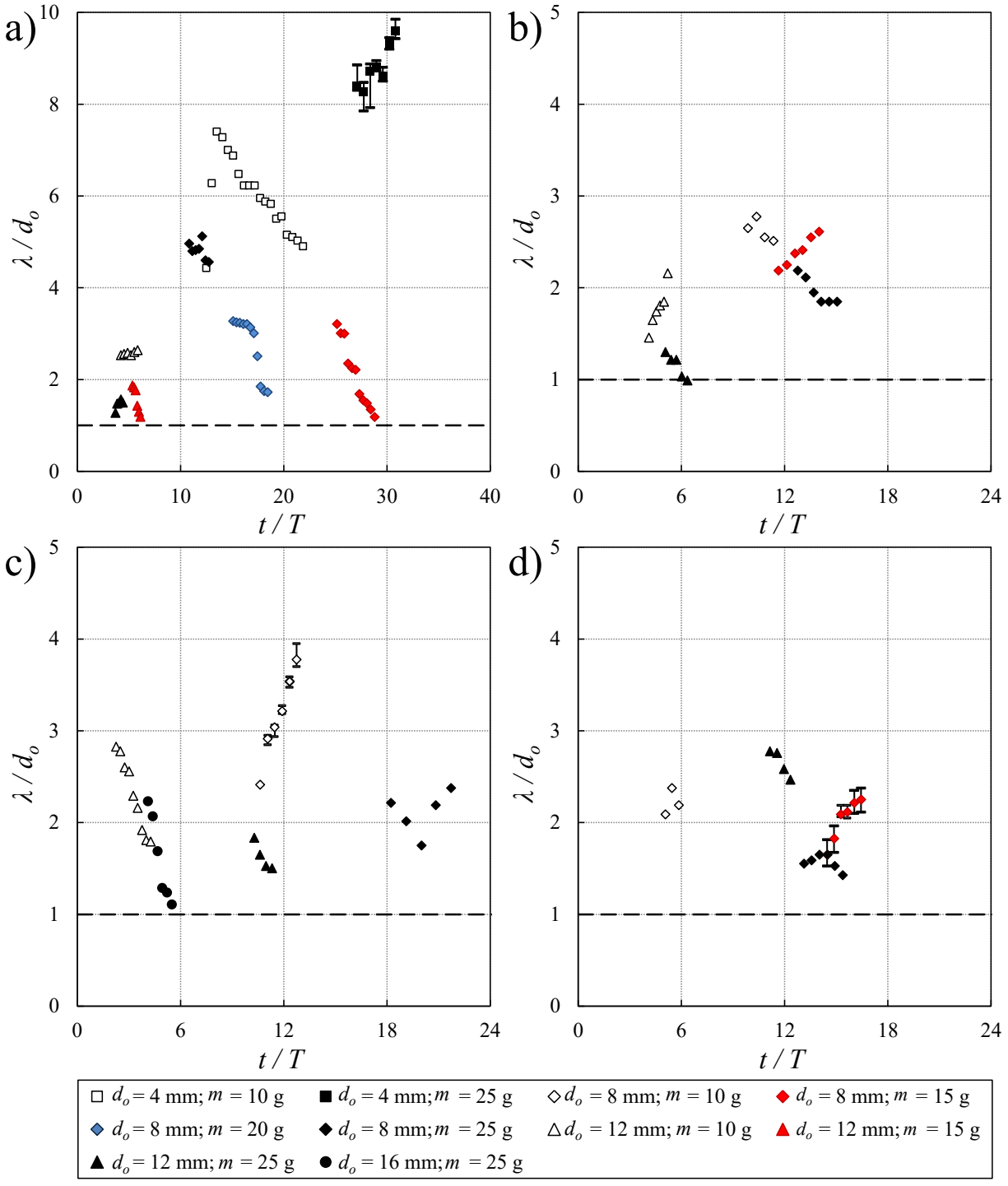


**Figure 3-9:** Variations of the wave length of the trailing part of sand jets $\lambda$ with non-dimensional time $t/T$ for different nozzle sizes and masses. a) $h_{oil}$=4 mm; b)$h_{oil}$=6 mm; c)$h_{oil}$=10 mm; d)$h_{oil}$=30 mm.

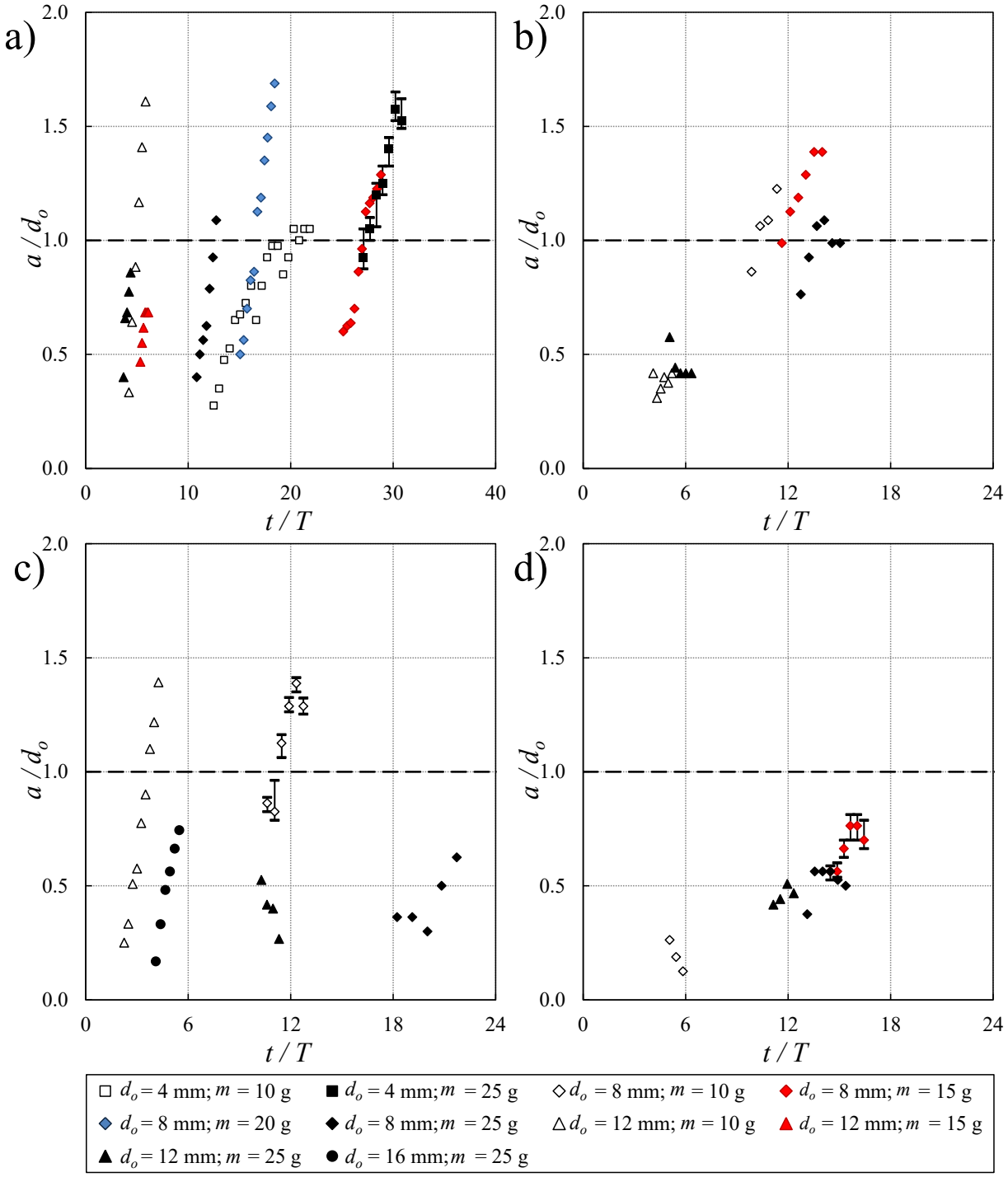


**Figure 3-10:** Variations of the amplitude of the trailing part of the sand jets $a$ with non-dimensional time $t/T$ for different nozzle sizes and masses. a) $h_{oil}$=4 mm; b) $h_{oil}$=6 mm; c) $h_{oil}$=10 mm; d) $h_{oil}$=30 mm.

Fig. 3-9a and 3-10a show the variations of $\lambda/d_o$ and $a/d_o$ with $t/T$ for $h_{oil}$=4 mm, respectively. As can be seen, in most cases the trailing wave compressed since the wavelength decreased while the amplitude of the wave increased. The trailing of the oily sand jet in this case was not strong enough to overcome the drag force exerted by the ambient water, therefore the wave was compressed. Strong wave instability was observed for oily sand jets with small oil layer. When the wave reaches the maximum penetration, it breaks down in smaller pieces. Wave growth can be observed from tests with thicker oil layer (i.e., $h_{oil}$=6 mm, $d_o$=8 mm, $m$=15 g). For those tests, both amplitude and wavelength increased with time. Figs. 3-9b and 3-10b show the wave dynamics of oily sand jet for $h_{oil}$=6 mm. Compression was observed for jets with larger particle mass whereas wave stretch was observed for jets with smaller mass (Test No. 18). Wave dynamics of oily sand jets passing through 10 mm of oil layer was shown in Figs. 3-9c and 3-10c.

Wave decay was observed for jets with large masses (Test No. 46) which both $a$ and $\lambda$ decreased. The magnitude and variations of wave characteristics for oily sand jets passing through thick oil layer ($h_{oil}$=30 mm) indicated that the thick oil layer damped the trailing wave. Considering oily sand jets with $d_o$=8 mm and $m$=10 g (i.e., open diamond) in Figs 3-9c and 3-9d indicated that the average wavelength dropped from $3.5d_o$ to $2.2d_o$. The average amplitude of the waves was also reduced from $1.2d_o$ to $0.25d_o$. No wave formation was observed for $d_o$=16 mm and in the present oil layer thickness ranges. When masses of particles passed through the largest nozzle, a ball was formed from the beginning of the test and it descended as a ball to the bottom. Therefore, no trail was formed because of bursting at the rear of the ball (see Fig. 3-5b).

## 3.5 Summary and Conclusions

Laboratory experiments were conducted to investigate the dynamics of sand jets passing through two immiscible liquids (i.e., oil and water). Effects of experimental parameters such as nozzle size, oil layer thickness and mass of sand particles on evolution of oily sand jets were studied in detail by comparing the images sand jet front at different times. Eight different shapes of oily sand jets were observed and frontal shapes were classified in two categories of stable and unstable jets. Stable jets were observed for smallest nozzle size ($d_o$=4 mm), and $h_{oil}$<30mm. Oily sand jets became unstable for 8 mm≤$d_o$≤16 mm. Once the frontal head of the oily sand jets becomes unstable the jet front oscillates and it bursts into small groups of particles. It was found that the effect of nozzle size was predominant and mass of sand particles did not control the stability of oily sand jets. Ball shape was observed mostly for the largest nozzle size ($d_o$=16 mm). Bursting of the frontal head was also occurred based on the oil layer thickness and mass of sand particles.

Effects of initial parameters on the growth of frontal widths $w_f$ were studied and experimental results were compared with the growth rate of water jets thermal of heavy salt. It was found that the growth rate is independent of the nozzle size. Oily sand jets became stable at the beginning of the test and they became unstable at a distance ten times larger than the nozzle diameter. This can be observed by sudden growth of frontal width for $x/d_o$≤10. Far from the nozzle ($x/d_o$>10), the width of frontal head linearly increased with $x/d_o$. Our observations of frontal width for jets with $m$=25 g indicated that excess momentum due to higher mass of sand particles increased the jet instability and caused higher frontal width. In these conditions, the growth rate became similar to the growth rate of a single-phase buoyant thermal. The evolution of oily sand jets in

water can be studied by measuring the variations of frontal velocities with time. Variations of the frontal velocities with distance along the jet indicated two envelopes of an acceleration followed by a deceleration. The acceleration and deceleration phases were interpreted based on the shapes of oily sand jets to describe the evolution of jets in water. The first acceleration phase was observed from the beginning of the test to $t/T$=3~6. Frontal velocities in this range increase by 20%−40% of the initial jet velocities. The deceleration phase occurred for $3<t/T<16$. The second acceleration and deceleration cycle will form once the hook or torsion shapes of front reached their maximum sizes. Second deceleration may be due to separation of oily sand jets into groups of sand particles and deviation of oily sand jets from vertical path. Our observations and measurements can be used to study the evolution of oily sand jets in an opaque medium.

The dynamics and mixing of particles in the ambient can be significantly altered by bursting of oily sand jets. Three various bursting mechanisms named as bifurcation bursting, rear bursting and multiple bursting were observed for $L/d_o$=32.6, $L/d_o$=1 and $L/d_o$ of 4.83, respectively. Study the variations of the normalized bursting time $t/T$ with $L/d_o$ for three different oil layer thicknesses indicated an adverse relationship between the normalized bursting time and nozzle diameter. It was found that nozzle diameter has a significant effect on bursting time and bursting time decreases as nozzle diameter increases. No bursting was observed for the smallest nozzle ($d_o$=4mm), since the frontal part splits into many small groups of particles. The shear stress of oily sand jets was measured and the effect of nozzle diameter on shear stress was studied. It was found that the nozzle diameter has a direct relationship with shear stress and the magnitude of the

shear stress is independent of $x/d_o$. It was found that the normalized shear stress is constant for all tests with a value of 0.16±0.01.

Variations of the amplitude $a$ and wavelength $\lambda$ of trailing waves at different times were studied. For cases that the trailing of the oily sand jets was not strong enough to overcome the drag force exerted by the ambient water, the wavelength decreased while the amplitude of the wave increased. Strong wave instability was observed for oily sand jets with small oil layer. For oily sand jets passing through thicker oil layer (i.e., $h_{oil}$=6 mm, $d_o$=8 mm, $m$=15 g) both amplitude and wavelength increased with time. Wave stretch and wave decay were observed for jets with small ($m$=10 g) and larger masses ($m$=25 g), respectively. The magnitude and variations of wave characteristics for oily sand jets passing through thick oil layer ($h_{oil}$=30 mm) indicated that thick oil layer damped the trailing wave. No trail and wave was formed for $d_o$=16 mm since bursting at the rear of the ball was occurred.

## 3.6 Notation

$a$ = Wave amplitude, mm

$A$= Projected area, $m^2$

B= Buoyancy flux, $m4/s^3$

$c_o$ = Initial volumetric concentration of particles, vol/vol

$d_o$= Nozzle diameter, mm

$D_{50}$ = particle size, mm

Fr= Froude number

$F_B$= Buoyancy force, N

$F_D$= Form drag force, Pa

$F_g$= Gravitational force, kg.m/s$^2$

$F_\tau$= Skin friction drag force, kg.m/s$^2$

$g$ = Acceleration due to gravity, m/s$^2$

$g'$=Reduced gravity, m/s$^2$

$h_{oil}$= Thickness of oil layer, mm

$L$ = Length of sand in release tube, mm

$L_M$= length scale

$M$= Momentum, m$^4$/s$^2$

$m$= Mass of sand particles, g

$Q$ = Flow rate, m$^3$/s

Re = Reynolds number

$Re_p$ = Particle Reynolds number

Ri = Richardson number

$t$ = Time, s

$\Delta t$ = Time interval, s

$T$ = Characteristic time scale, s

$u_f$ = Frontal velocity of oily sand jet, mm/s

$u_o$ = Initial velocity of oily sand jet, mm/s

$u_\infty$ = Terminal settling velocity, mm/s

$w_f$ =Width of oily sand jet, mm

$x$ =Frontal position from the nozzle, mm

$\alpha$ = Coefficient

$\lambda$ = Wavelength of the trailing jet, mm

$\mu_l$= Dynamic viscosity of water, $kg.m^{-1}.s^{-1}$

$\mu_{oil}$= Dynamic viscosity of canola oil, $kg.m^{-1}.s^{-1}$

$\rho_{oil}$ = Density of Canola oil, $kg/m^3$

$\rho_s$ = Density of sand, $kg/m^3$

$\rho_w$ = Density of water, $kg/m^3$

$\tau$ = Shear stress, Pa

## Chapter 4

# Modeling for Oily Sand Jets by Using Weka Software

## 4.1 Introduction

Knowledge Discovery in Data (KDD) or data mining is a computational process to extract meaningful patterns and rules from a large number of variables and data using Weka software.

Weka software written in Java language and it has a collection of machine learning algorithms to extract the relationship between different parameters (Weka, 2013). The classifiers in Weka enable to prepare classification, regression algorithms and estimate the accuracy of the proposed model (Witten and Frank, 2005). Different classifiers were implemented in Weka for data classification named as Bayesian, Trees, Rules, Functions and Lazy classifiers (Witten and Frank, 2005). Attributes in classifiers are categorized into numeric and nominal. Numeric attributes are variables such as time and nominal attributes can be defined to be certain such as nozzle diameter, oil layer thickness or they can be different shapes of oily sand jets in water (i.e., ball shape, hook shape).

NaiveBayes is one of the classifiers in Bayes package which has been used as an estimator in the past (Witten and Frank, 2005). This classifier improves the performance of simulation if the normality assumption for data is extremely incorrect. The main idea of the Bayes's rule is that the outcome of an event $H$ can be predicted based on some evidences $E$ that can be observed as

$$P(H \mid E) = \frac{P(E \mid H) \times P(H)}{P(E)} \tag{1}$$

The normal distribution and completely independent assumptions for numeric attributes are restrictions of the NaiveBayes classifier (Witten and Frank, 2005). J48 is a standard algorithm that is widely used for practical machine learning and produces decision tree models.

The main goal of the model tree approach is the process of dividing complex problems into smaller problems (Bhattacharya et al., 2007). Model trees are accurate, understandable, and easy to train and it can be employed as a robust method for classification, prediction and dealing with missing data (Witten and Frank, 2005; Jung et al. 2010). One of the most famous approaches of model tree simulation is M5 algorithm which was initially introduced by Quinlan (1992). Two main procedures are involved in the algorithm as building the tree and inferring knowledge from it (Jung et al., 2010; Etemad-Shahidi et al., 2010). M5P is an improved version of the M5 algorithm which is proposed by Wang and Witten (1997). The new version has a similar structure to the M5 algorithm which produces easier trees and effectively deals with missing values and enumerated attributes (Jung et al., 2010; Etemad-Shahidi et al., 2010). The M5P algorithm generally consists of three main steps as building the tree, pruning the tree and smoothing it. One distinct advantage of this mechanism is more transparent than other machine learning algorithms such as artificial neural network (ANN), *k* nearest neighbouring (*k*NN) and logistic regression. Therefore, it is easy to follow a tree structure to understand how a decision has been made (Pedrycz and Sosnowski, 2001). Other advantages of model trees are that they are more accurate than ANN, easy to train and robust when dealing with missing data (Witten and Frank, 2005). This study is organized in 4 sections. In section 4.2 experimental setup and modeling are discussed. Results and

data mining techniques such as model tree are discussed in section 4.3. Summary and conclusions of the present study is explained in section 4.4.

## 4.2 Setup and Modeling

In this study, explorer application and pre-processing for 740 data was used to understand evolution of oily sand jet front and classify the shapes of the frontal jets. Ten data sets for $x$, $w_f$, and $u_f$ were extracted from 74 experimental tests with a time interval of 0.1 second. All experiment details are listed in Table 3-1. In this study the NaiveBayes classifier used which build obvious and clear boundaries between different shapes of the oily sand jets and M5P method is tested to visualize trees for distance $x$, width $w_f$, and frontal velocity $u_f$ of oily sand jets.

## 4.3 Data Mining Modeling and Results

Two data sets were used for model training known as set #1 and model testing known as set #2. Those sets of data were collected from repeated experimental tests. Fig. 4-1 illustrates the histograms of various shapes, distances from the nozzle $x$, widths $w_f$ and frontal velocities of the oily sand jet $u_f$ for training and testing sets of data. Approximately 34.6% of shapes in oily sand jets have separation in water ambient for set #1 whereas the bursting shape has the maximum frequency of 37.7% in set #2 (see Fig. 4-1a). This difference may be related to the selection of time interval (i.e., $\Delta$t=0.1 s) and uncertainties of experiments. This figure also shows that other shapes of oily sand jets such as bar, hook, wave and ball shapes have similar frequencies in both sets.

Fig. 4-1b shows that about 80% of $x$ measurements are less than 200 mm. In other words when most particles pass through the nozzle, they either separated or burst at $x$<200 mm

and only ball or bar shapes reached the bottom of the tank. The histogram of sand jet width $w_f$ implied that the width can be classified into narrow jets ($w_f$<30) to very wide oily sand jets ($w_f$>90) (see Fig. 4-1c).

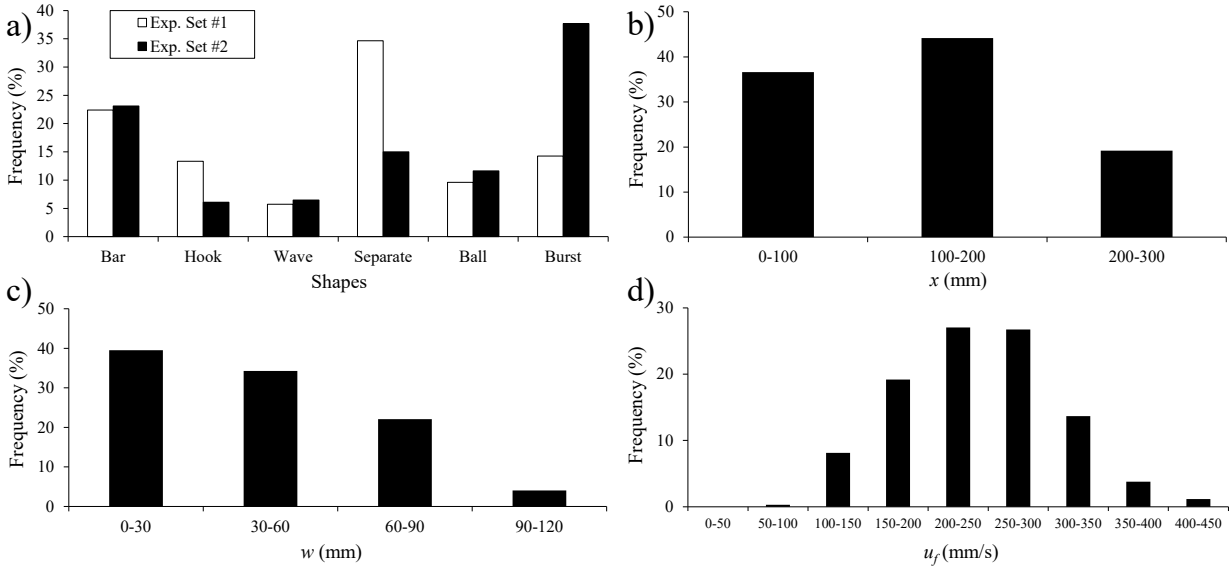


**Figure 4-1:** Histograms of the sand-jets parameters using by Weka software; a) Histogram of shapes; b) Histogram of distance from nozzle; c) Histogram of the width of sand-jets; d) Histogram of the frontal velocity.

The maximum and minimum frequencies are related to narrow jets and very wide jets with 40% and 5% frequencies, respectively. Fig. 4-1d shows the histogram of frontal velocity of oily sand jets. 53.77% of data have the frontal velocity range of 200 mm/s≤$u_f$≤300 mm/s. It is noticeable that the highest frontal velocity range (400 mm/s≤$u_f$≤450 mm/s) has the lowest frequency of about 2%.

### *4.3.1- Model Classification*

Understanding the effect of mass and oil layer thickness on evolution of oily sand jets and shape formation such as bar, hook, wave, ball, separation and burst shapes is essential. The NaiveBayes classifier in bayes category was used for boundary

visualization using Weka software (Weka, 2013). In this study, 740 data were used for boundary maps of various shapes and 344 data were used for classification of $x$ and $w_f$. Fig. 4-2 shows the boundary maps to determine the shapes of oily sand jets with time. Mass and oil layer thickness were normalized in form of $L/d_o$ and $h_{oil}/d_o$.

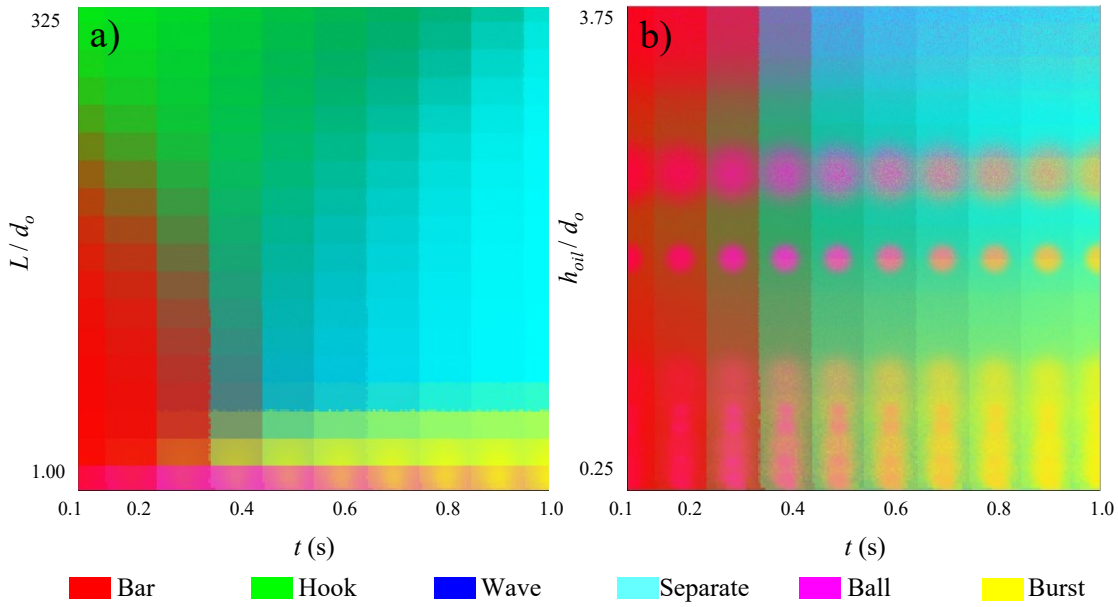


**Figure 4-2:** Boundary maps of various shapes of sand jets passing through an oil layer at different times. NaiveBayes model was used for boundary classification of Weka software. a) Effect of the normalized mass $L/d_o$ on the sand-jets classification. b) Effect of the normalized oil layer thickness $h_{oil}/d_o$ on the sand-jets classification.

As can be seen from Fig. 4-2a, bar shape was formed for $L/d_o$<130 and $t$< 0.2 s and ball shape was formed for $L/d_o$<3 and $t$< 0.7 s. A ball shape can be formed at the onset of the experiment if small amount of particles pass through a large nozzle (i.e., small $L/d_o$) while for large masses ($m$> 5g) and small nozzle ($d_o$<16 mm) a bar shape can be formed. For larger $L/d_o$ and longer time the bar shape was turned into a hook. The green area in Fig. 4-2a clearly shows the condition of hook formation. The narrow area in yellow shows the rear bursting occurs for jets with small $L/d_o$ and the large area in light blue

shows the separation other forms. This shape can be formed for large masses and small nozzle diameters (i.e., Test No.16). Fig. 4-2b shows the effect of oil layer thickness on the shapes of oily sand jets. As can be seen, formation of bar shape was independent of oil layer and it turned to other shapes for $t$>0.2 s. Formation of many circles at certain $h_{oil}/d_o$ in boundary map indicated a noise in data. It means that the shapes of oily sand jets are not only a function of $h_{oil}/d_o$ and they may depend on other parameters as well. The hook shape is formed for 1/4<$h_{oil}/d_o$<3/8 therefore no hook shape formed for thick oil layer and large nozzle (i.e., Test No.71). The burst and separation were formed at the larger times. The distinct difference between these two shapes is due to oil layer thicknesses and nozzle diameter. The former happened for thin oil layers ($h_{oil}/d_o$<3/8) and the latter happened for thick oil layers ($h_{oil}/d_o$>1/4).

A range of variables affect the frontal position and width of oily sand jets. Two important variables are nozzle diameter and oil layer thickness. Performance of Weka on classification of oily sand jets using two variables of $x$ and $w_f$ are shown at Fig. 4-3. The J48 classifier in trees model category was used for boundary visualization using Weka software. Fig. 4-3a shows the effect of nozzle diameter on $x$ with time. Frontal positions were divided into three classes. This boundary map can be used to estimate the average velocity of the front in each class. As can be seen in Fig. 4-3a, oily sand jets with small nozzle diameter ($d_o$=4 mm) reached $x$=100 mm at $t$=0.6 s whereas for jets with larger nozzle size ($d_o$= 16 mm) this time was 0.2 s. Fig. 4-3b shows the model results on classification of oily sand jets based on oil layer thickness and time. It is expected that the jets decelerated by increasing the oil layer thickness. Since the position of the frontal

head was also function of mass and nozzle diameter, boundary map showed some data scatter for higher oil layer thicknesses.

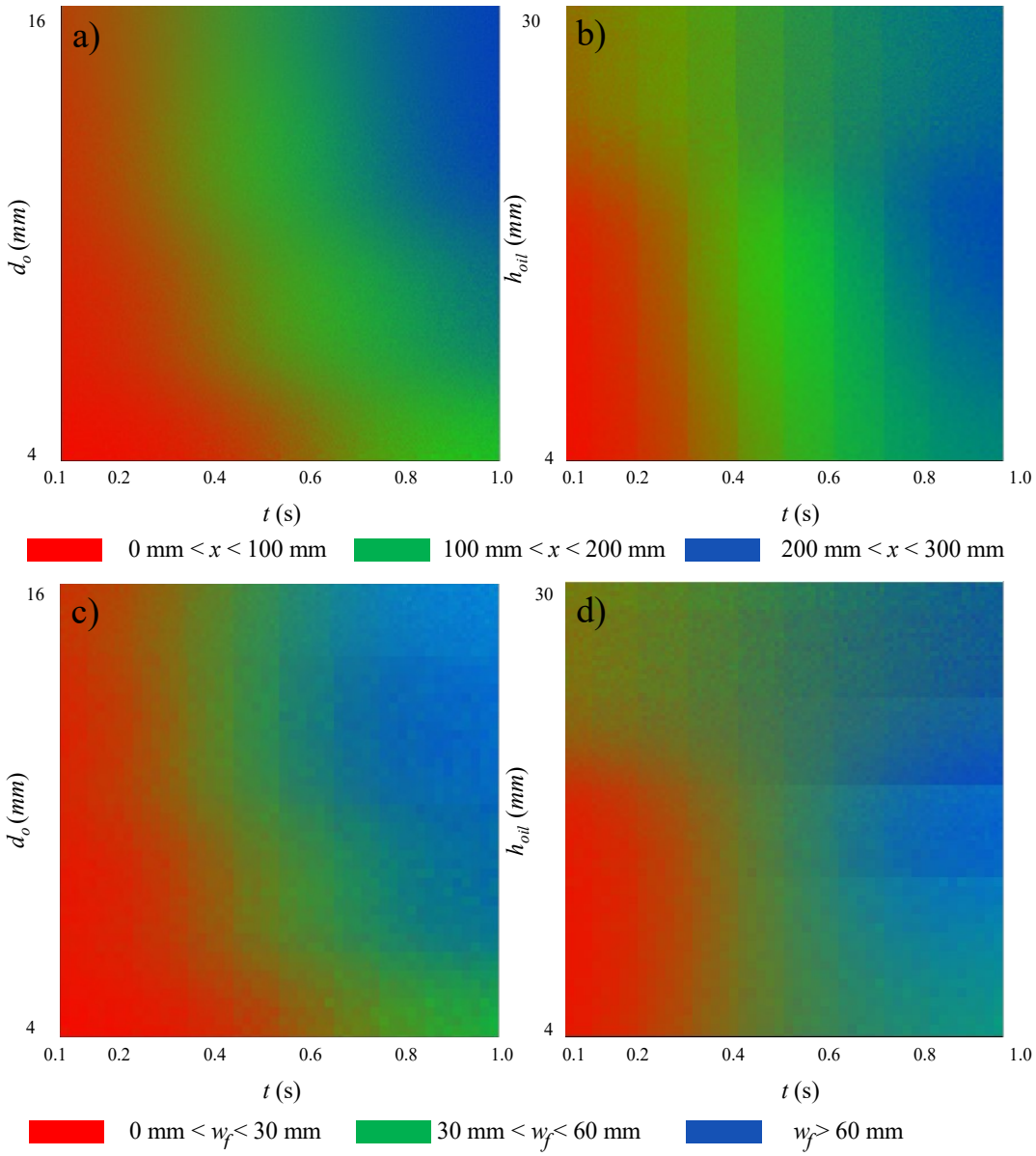


**Figure 4-3:** Visualization of boundary for distance $x$ and width $w_f$ of sand jets. J48 model was used for boundary classification a) Effect of nozzle diameter $d_o$ on $x$; b) Effect of oil layer thickness $h_{oil}$ on $x$; c) Effect of nozzle diameter $d_o$ on $w_f$; d) Effect of oil layer thickness $h_{oil}$ on $w_f$.

As can be seen, frontal position can descend even further in the region of high oil layer (i.e., blue area) whereas for jets with thin oil layer, the frontal head either bifurcated or burst before reaching the bottom. This can be due to formation of large ball for tests with high sand masses. Fig. 4-3c and 4-3d show boundary plots of the width of oily sand jets considering nozzle diameter and oil layer thickness with time, respectively. As can be seen from Fig. 4-3c, $w_f$ increased up to 30 mm for $d_o$=4 mm at $t$<0.6 s whereas the width growth for $d_o$=16 mm occurred at $t$<0.3 s. However, the width of oily sand jets did not grow more than 60 mm for $d_o$=4, 8 mm. Similarly, boundary plot in Fig. 4-3d shows the effect of $h_{oil}$ and time on $w_f$.

### *4.3.2- Model tree*

Fig. 4-4 shows the structure of the model tree for $x$, $w_f$, and $u_f$ constructed by M5P and linear models. The proposed linear model to predict $x$, $w_f$, and $u_f$ are listed in Table 4-1. Time was found to be the attribute that maximizes the expected error reduction. Fig. 4-4a, shows the tree model structure for prediction of $x$ using two linear models and time-attribute split at $t$=0.45. Structure of model tree for prediction of $w_f$ required four linear models.

**Table 4-1:** Performance of M5P classification model in form of a series of linear models (LM=$\eta_1 \times h_{oil}+\eta_2 \times d_o+\eta_3 \times m+\eta_4 \times t+C$) to predict $x$, $w_f$, and $u_f$.

| Parameter | Linear model | $\eta_1$ | $\eta_2$ | $\eta_3$ | $\eta_4$ | $C$ |
|---|---|---|---|---|---|---|
| $x$ | LM1 | 0.82 | 3.66 | −0.02 | 257.6 | 41.6 |
| | LM2 | 1.01 | 7.94 | −0.30 | 211.5 | −64.8 |
| $w_f$ | LM1 | 0.39 | 1.32 | 0.02 | 61.9 | −13.3 |
| | LM2 | 0.76 | 2.97 | 0.35 | 62.3 | −35.0 |
| | LM3 | 0.13 | 1.73 | 0.08 | 82.1 | −20.9 |

| | | | | | | |
|---|---|---|---|---|---|---|
| | LM4 | 0.0 | −0.27 | 2.25 | 82.6 | −30.9 |
| $u_f$ | LM1 | 0.0 | 4.25 | −0.45 | 29.1 | 133.4 |
| | LM2 | 0.0 | 2.83 | −2.72 | -3.2 | 245.5 |
| | LM3 | 0.0 | −0.73 | 0.41 | -162.4 | 337.3 |
| | LM4 | 0.0 | 10.68 | 0.41 | -45.5 | 171.2 |
| | LM5 | 0.0 | 1.78 | -0.22 | 23.4 | 231.7 |
| | LM6 | 0.0 | 8.70 | -0.22 | -4.9 | 144.7 |

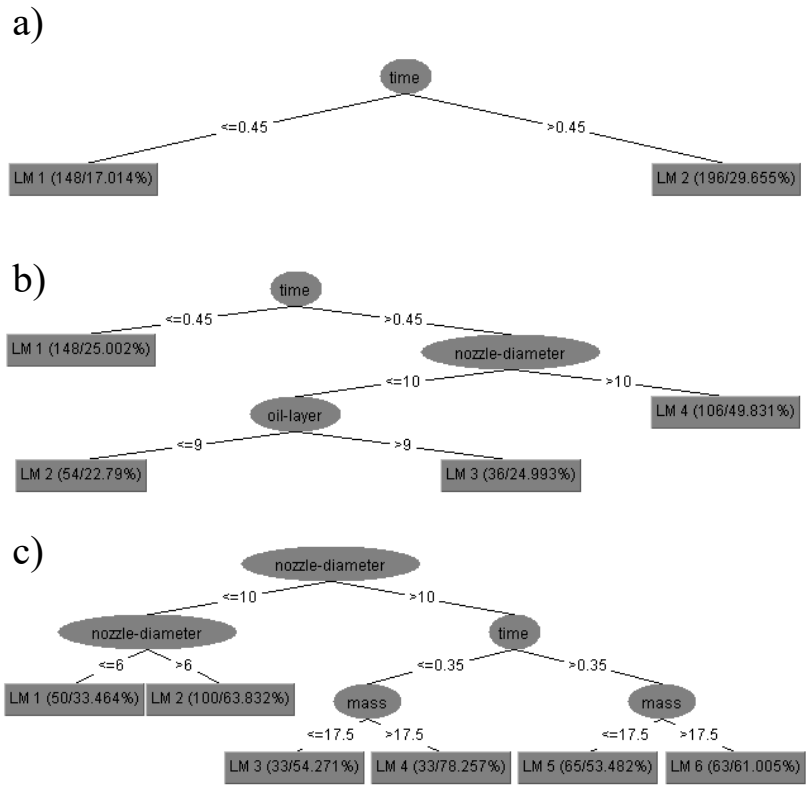


**Figure 4-4:** Structure of model trees constructed by M5P and linear models for $h_{oil}$=4, 6, 8, 10, 12, 30 mm, $d_o$=4, 8, 12, 16 mm and $m$=10, 25g.a) Model tree for $x$; b) Model tree for $w_f$; c) Model tree for $u_f$.

As can be seen in Fig. 4-4b, time-attribute was the most important parameter of classification and the effects of nozzle size and oil layer thickness became important for $t$>0.45 s. Nozzle diameter of $d_o$=10 mm and $h_{oil}$=9 mm were found to be critical for classification of $w_f$. Model tree results for prediction of frontal velocities indicated that the nozzle size was the main criterion of classification. Weka proposed six linear models to estimate $u_f$ (LM1-LM6). As can be seen from Fig. 4-4c, $u_f$ is independent of time for $d_o$<10 mm. For $d_o$>10 mm, M5P model showed that both time and mass were important for prediction of $u_f$. Here the time considered as an attribute to split due to various definition. The critical time and mass were 0.35 s and 17.5 g, respectively.

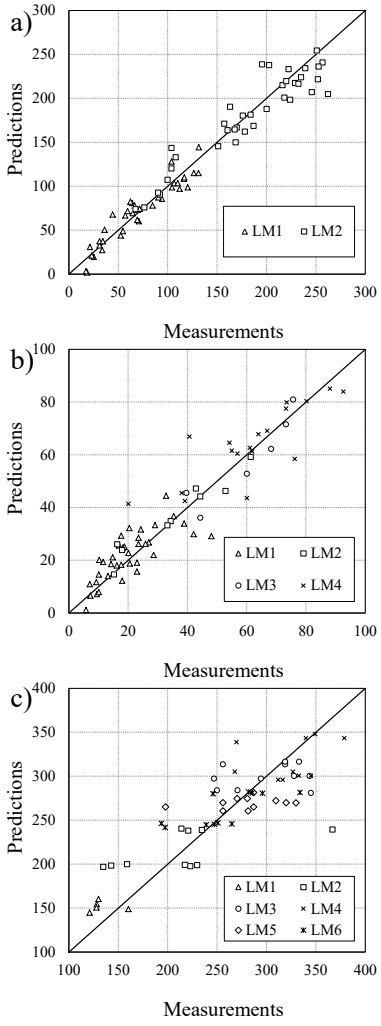

**Figure 4-5:** Comparison between laboratory measurements and prediction of Weka software. a) Prediction of $x$ by using two linear model; b) Prediction of $w_f$ by using four linear models; c) Prediction of $u_f$ by using six linear.

Figs. 4-5a-4-5c show a comparison between the laboratory measurements and predictions of Weka for $x$, $w_f$, and $u_f$, respectively. Proposed linear models for prediction of $x$ were found to be accurate with an average error of ± 8.2%. Considering the proposed linear models for prediction of $w_f$, M5P provided approximately more accurate predictions for LM2 and LM3 with average uncertainties of ± 3.3% and ± 5.7%, respectively. The overall uncertainty of prediction for $w_f$ and $u_f$ were ±6.8% and ±8.7%, respectively.

## 4.4 Summary and Conclusions

NaiveBayes classifier was used for boundary visualization. It was found that a ball shape can be formed at the onset of the experiment if small amount of particles pass through a large nozzle for $L/d_o<3$ and $t< 0.7$ s while for large masses ($m> 5$g) and small nozzle ($d_o<16$ mm) a bar shape can be formed. Study boundary map of oil layer thickness and shapes of oily sand jets indicated that the shapes of oily sand jets are not only a function of $h_{oil}/d_o$. Effects of two important variables were found on the frontal position and width of oily sand jets. The J48 classifier was used for boundary visualization to show the effect of nozzle diameter and oil layer thickness on $w_f$ and $u_f$. Model trees for simulation of $x$, $w_f$, and $u_f$ were constructed by M5P. Attributes were selected based on maximizing the expected error reduction. Two, four and six linear models were proposed to simulate $x$, $w_f$, and $u_f$. A comparison was made between laboratory measurements and simulation results. Proposed linear models for prediction of $x$ were found to be accurate with an average error of ± 8.2%.

## 4.5 Notation

$d_o$= Nozzle diameter, mm

$E$ = Evidence

$h_{oil}$= Thickness of oil layer, mm

$H$ = Outcome of an event

$L$ = Length of sand in release tube, mm

$m$= Mass of sand particles, g

$t$ = Time, s

$\Delta t$ = Time interval, s

$u_f$ = Frontal velocity of oily sand jet, mm/s

$w_f$ =Width of oily sand jet, mm

$x$ =Frontal position from the nozzle, mm

$\eta$ = coefficient of linear models

# Chapter 5

# General Conclusions and Recommendations for Future Research

## 5.1 General Conclusions

In the preceding chapters, the analysis and results of the laboratory experiments and modeling of data were presented on the dynamics of oily sand jets.

In chapter 3, the behaviour of sand jets front passing through two immiscible liquids with different nozzle diameters, oil layer thickness and mass of sand particles were investigated by using laboratory experiments. Effects of experimental parameters were studied in detail by comparing the images sand jet front at different time. It was found that nozzle diameter can significantly change the frontal shapes of the jets more than other parameters. The obtained results of this chapter can be employed for designing and for optimizing the onset of mixing systems. In this experimental study the following results were found:

- The frontal shape and its formation were classified into two categories which the nozzle diameter $d_o$ was the parameter of classification.
- The growth rate of frontal widths $w_f$ was independent of the nozzle size.
- Oily sand jets became stable at the beginning of the test and they became unstable at a distance ten times larger than the nozzle diameter.
- Frontal width for jets with $m$=25 g indicated that excess momentum due to higher mass of sand particles increased the jet instability and caused higher frontal width.

- The growth rate became similar to the growth rate of a single-phase buoyant thermal for jets with $m$=25 g.
- Variations of the frontal velocities with distance along the jet indicated two envelopes of an acceleration followed by a deceleration.
- Frontal velocities from the beginning of the experiment to $t/T$=3~6 increase 20%−40% of the initial jet velocities.
- Once the hook or torsion shapes of front reached their maximum sizes, the second acceleration and deceleration cycle for frontal velocity was formed.
- Three various bursting mechanisms named as bifurcation bursting, rear bursting and multiple bursting were observed for $L/d_o$=32.6, $L/d_o$=1 and $L/d_o$ of 4.83, respectively.
- An adverse relationship was found between the normalized bursting time $t/T$ and nozzle diameter $d_o$ for three different oil layer.
- There was not any bursting for the smallest nozzle size ($d_o$=4mm), since the frontal part splits into many small groups of particles.
- The nozzle diameter had a direct relationship with shear stress and the magnitude of the shear stress is independent of $x/d_o$.
- The value of normalized shear stress was constant for all tests about 0.16±0.01.
- Strong wave instability was observed for oily sand jets with small oil layer. Wave stretch and wave decay were observed for jets with small ($m$=10 g) and larger masses ($m$=25 g), respectively.
- The thick oil layer ($h_{oil}$=30 mm) damped the trailing wave and wave was not formed for $d_o$=16mm.

In chapter 4, data mining and boundary visualization techniques were used to study the effects of experimental parameters on the shapes of oily sand jets. Model trees were developed to classify and predict the growth of oily sand jets at different conditions. Following results were found in Chapter 4.

- About 80% particles passed through the nozzle, they either separated or burst at $x$<200 mm and only ball or bar shapes reached the bottom of the tank.
- The histogram of sand jet width $w_f$ implied that the width can be classified into narrow jets ($w_f$<30) to very wide oily sand jets ($w_f$>90).
- The shapes of oily sand jets were not only a function of $h_{oil}/d_o$ by study boundary map of oil layer thickness and shapes of oily sand jets by using NaiveBayes classifier.
- Structure of model tree for prediction of $x$, $w_f$ and $u_f$ required two, four and six linear models, respectively.
- The model tree classified based on critical parameters.
- The model tree predicted the growth of sand jets with an uncertainty of ±8.2%, ±6.8% and ±8.7% for width, velocity and distance, respectively.

## 5.2 Future Research Studies

This research can be expanded in several ways. In this thesis, the effect of various parameters such as nozzle diameter, oil layer thickness and mass of sand particles investigated on dynamics of oily sand jets. Particle size is one of the parameters can have significant effect on axial velocity and frontal width of the sand jet. Another parameter can be considered in future is release height. Different release height might be changed shape and velocity of the sand jets. It is generally known

that jets and plumes entrain the surrounding fluid. Both sand-phase and water-phase mass fluxes and the entrainment coefficient can be calculated.

## References


Arakeri, J. H., Das, D., Krothapalli, A., and Lourenco L. (2004). "Vortex ring formation at the open end of a shock tube: A particle image velocimetry study." *Physics of Fluids*, 16, 4, 1008–1019.

Azimi, A., Zhu, D. Z., and Rajaratnam, N. (2012a). "Experimental study of sand jet front in water."*J. Multiphase Flow*. 40, 19–37.

Azimi, A., Zhu, D. Z., and Rajaratnam, N. (2012b). "Computational investigation on verticalslurry jets." *Int. J. Multiphase Flow*. 47, 94–114.

Azimi, A. H., Zhu, D. Z., Rajaratnam, N. (2014). "Experimental Study of Subaqueous Sand Deposition from Slurry Wall Jets" *J. Eng. Mech*., 140, 296–314.

Azimi, A. H., Zhu, D. Z., Rajaratnam, N. (2015). "An experimental study of circular sand–water wall jets" *Int. J. Multiphase Flow*, 74, 34–44.

Baines, W. D. (1975). "Entrainment by a plume or jet at a density interface." *J. Fluid Mech*. 68, 309–320.

Bhattacharya, B., Price, R. K., and Solomatine, D. P. (2007). "Machine learning approach to modeling sediment transport."*J. Hydraul. Eng*. 133(4), 440–450.

Bond, D., Johari, H. (2005). "Effect of initial geometry on the development of thermals" *Exp*. *Fluids* 39, 589–599.

Bond, D., and Johari, H. (2010). "Impact of buoyancy on vortex ring development in the near field." *Experiment in Fluids*, 48, 737–745.

Brush, L. M. J. (1962). "Exploratory study of sediment diffusion." *J. Geophys. Res*. 67(4), 1427–1433.

Buhler, J., and Papantoniou, D. A. (1991). “Swarms of coarse particles falling through a fluid.” *In Environmental Hydraulics* (ed. J. T. Lee & T. K. Cheung), 135–140. Balkema, Rotterdam.

Bush, J.W.M., Thurber, B.A., Blanchette, F. (2003). “Particle clouds in homogeneous and stratified environments”. *J. Fluid Mech*. 489, 29–54.

Cai, J., Zhu, D. Z., and Rajaratnam, N. (2012). “Observations on sand jets in viscoplastic fluids.” *Theoretical & applied mechanics letters,*2,052001.

Cai, J., Hall, N., Elenany, M., Zhu, D. Z., and Rajaratnam, N. (2010). “Observations on sand jets in air.” *J. Mech. Eng*. 136 (9), 1181–1186.

Carazzo Guillaume, Jellinek. A. Mark. (2012). “A new view of dynamics, stability and longevity of volcanic clouds.” *Earth and Planetary Science Letters*. 325–326, 39–51.

Etemad-Shahidi, A., Taghipour, M. (2010). “Predicting longitudinal dispersion coefficient in natural streams using M5 model tree.” *J. Hydraulic Eng*. 138(6), 542–554.

Fischer, H. B., List, E. J., Koh, R. C. Y., Imberger, J., and Brooks , N. H. (1979). “Mixing in inland and coastal waters.” Academic, London.

Fridman, P. D., Katz, J. (2000). “Rise height for negatively buoyant fountains and depth of penetration for negatively buoyant jets impinging an interface.” *J. Fluids*. *Eng*. 122, 779–782.

Fridman, P. D., Katz, J. (1999). “The flow and mixing mechanisms caused by the impingement of an immiscible interface with a vertical jet.” *J. Phys*. *Fluid*. 11(9), 2598–2606.

Geyer, A., Phillips, J. C., Mier-Torrecilla, M., Idelsohn, S. R., and Onate, E. (2011). “Flow behaviour of negatively buoyant jets in immiscible ambient fluid.” *Exp. Fluids*. 52, 261 271.

Gharib, M., Rambod, E., and Shariff, K. (1998). “A universal time scale for vortex ring formation.” *Journal of Fluid Mechanics*, 360, 121–140.

Giraut, F., Carazzo, G., Tait, S., Ferrucci, F., and Kaminski, E. (2014). “The effect of total grain-size distribution on the dynamics of turbulent volcanic plumes.” *Earth and Planetary Science Letters*. 394, 124–134.

Hall, N., Elenany, M., Zhu, D. Z., and Rajaratnam, N. (2010). “Experimental study of sand and slurry jets in water.” *J. Hydraulic Eng*. 136(10), 727–738.

Jiang, J. S., Law, A. W. K., Cheng, N. S. (2005). “Two-phase analysis of vertical sediment-laden jets.” *Journal of Eng. Mechanics*, 131(3), 308-318.

Jung, N. C., Popescu, I., Keldeman, P., Solomatine, D. P., and Price, R. K. (2010). “Application of model trees and other machine learning techniques for algal growth prediction in Yongdam reservoir, Republic of Korea.” *J. Hydroinf*. 12(3), 262–274.

Krueger, P. S., and Gharib M. (2003). “The significance of vortex ring formation to the impulse and thrust of a starting jet.” *Physics of Fluids*, Vol. 15, 4, 1271-1281.

Lee, J. H. W., Chu, V. H. (2003). “Turbulent jets and plums, A Lagrangian Approach.”*Kluwer Academic Publishers Group*, The Netherlands, 390p.

Mazurek, K. A., Christison, K., and Rajaratnam, N. (2002). “Turbulent sand jet in water.”*J. Hydraulic. Res.* 40(4), 527–530.

Metzger, B., Nicolas, M., and Guazzelli, E. (2007). “Falling clouds of particles in viscous fluids.” *J. Fluid Mech*. 580, 283–301.

Nicolas, M. (2002). “Experimental study of gravity-driven dense suspension jets.” *J. Phys*. *Fluids*. 14(10), 3570–3576.

Noh, Y. (2000). “Sedimentation of a particle cloud across a density interface” *Fluid Dyn. Res.*, 27, 129–142.

Noh, Y., Fernando, H.J.S. (1993). “The transition in the sedimentation pattern of a particle cloud” *Physics of Fluids A: Fluid Dynamics, 5,* 12, 3049–3055.

Noh, Y., Fernando, H.J.S., and Ching, C. Y. (1992). “Flows induced by the impingement of a two dimensional thermal on a density interface.” *J. Physical Oceanography.*22, 1207-1220.

Pantzlaff, L. & Lueptow, R. M. (1999). “Transient positively and negatively buoyant turbulent round jets.” *Experiments in Fluids*, 27, 117-125.

Pedrycz, W., and Sosnowski, Z. A. (2001). “The design of decision trees in the frame work of granular data and their application to software quality models.” *Fuzzy Sets Syst*. 123, 271–290.

Philippe, P., Raufaste, C., Kurowski, P., and Petitjeans P. (2005). “Penetration of a negatively buoyant jet in a miscible liquid.” *J. Physics of Fluids*. 17, 053601.

Pignatel, F., Nicolas, M., and Guazzelli, E. (2011). “A falling cloud of particles at a small but finite Reynolds number.” *J. Fluid Mech*. 671, 34–51.

Pottebaum, T. S., and Gharib, M. (2004). “The pinch-off process in a starting buoyant plume.” Experiments in Fluids, 37, 87–94.

Quinlan, J. R. (1992). “Learning with continuous classes.” *Proc., 5th Australian Joint Conf. on Artificial Intelligence*, World Scientific, Singapore, 343–348.

Rahimipour, H. and Wilkinson, D. (1992). “Dynamic behavior of particle clouds” *Eleventh Australasian Fluid Mechanics Conference,* Vols 1 and 2, University of Tasmania, Hobart, Australia, 743–746.

Rao, K. K., and Nott, P. R. (2008). “An introduction to granular flow.” Cambridge University Press, Cambridge, N.Y.

Rogers, C. Michael and Morris. W. Stephen. (2009). “Natural versus forced convection in laminar starting plumes.” *J. physics of Fluids*. 21, 601–607.

Ruggaber, G. J. (2000). “Dynamics of particle clouds related to open-water sediment disposal.” *Ph.D. Thesis*, Dept. of Civil and Environmental Engineering, MIT, Cambridge, MA, 242 p.

Sheen, H. J., Jou, B. H., Lee, Y. T. (1994). “Effect of particle size on a two-phase turbulent jet.” *Experimental Thermal and Fluid Science*, 8, 315–327.

Singamsetti, S. R. (1966). “Diffusion of sediment in submerged jet.” *J. Hydr. Div*. 92(2), 153–168.

Turner, J. S. (1969). “Buoyant plumes and thermals.” *Annu. Rev. Fluid Mech*. 1, 29–44.

Virdung, T., Rasmuson, A. (2007). “Hydrodynamic properties of a turbulent confined solid-liquid jet evaluated using PIV and CFD.” Chemical Engineering Science, 62, 5963–5979.

Wang, Y., and Witten, I. H. (1997). “Induction of model trees for predicting continues classes.” *Proc. of the Poster Papers of the European Conf. on Machine*

*Learning*, 1997, Univ. of Economics, Faculty of Informatics and Statistics, Prague, Czech Republic.

Webster, D. R., and Longmire, E. K. (2001). "Jet pinch-off and drop formation in immiscible liquid-liquid systems." *Exp in Fluids*.30, 47–56.

Williamson, N., Srinarayana, N., Armfield, S. W., McBain, G. D., and Lin, W. (2008) "Low-Reynolds-number fountain behaviour." *J. Fluid Mech*. 608, 297–317.

Witten, I. H., Frank, E. (2005). "Data mining-Practical machine learning tools and techniques." Morgan Kaufmann, San Francisco.

Zhao, Bing., Law, W. K. Adrian., Adams, Eric., Shao, Dongdong., Huang, Zhenhua. (2012). "Effect of air release height on the formation of sediment thermals in water." *J. Hydraulic Research*. 50, 532–540.